Cell type-specific driver lines targeting the *Drosophila* central complex and their use to investigate neuropeptide expression and sleep regulation.

Tanya Wolff[1], Mark Eddison[1], Nan Chen[1], Aljoscha Nern[1], Preeti Sundaramurthi[2], Divya Sitaraman[2] and Gerald M Rubin[1#]

[1]Janelia Research Campus, Howard Hughes Medical Institute, Ashburn VA 20147
[2]Department of Psychology, College of Science, California State University, Hayward, California 94542
[#]Corresponding Author: rubing@janelia.hhmi.org

Abstract

The central complex (CX) plays a key role in many higher-order functions of the insect brain including navigation and activity regulation. Genetic tools for manipulating individual cell types, and knowledge of what neurotransmitters and neuromodulators they express, will be required to gain mechanistic understanding of how these functions are implemented. We generated and characterized split-GAL4 driver lines that express in individual or small subsets of about half of CX cell types. We surveyed neuropeptide and neuropeptide receptor expression in the central brain using fluorescent *in situ* hybridization. About half of the neuropeptides we examined were expressed in only a few cells, while the rest were expressed in dozens to hundreds of cells. Neuropeptide receptors were expressed more broadly and at lower levels. Using our GAL4 drivers to mark individual cell types, we found that 51 of the 85 CX cell types we examined expressed at least one neuropeptide and 21 expressed multiple neuropeptides. Surprisingly, all co-expressed a small neurotransmitter. Finally, we used our driver lines to identify CX cell types whose activation affects sleep, and identified other central brain cell types that link the circadian clock to the CX. The well-characterized genetic tools and information on neuropeptide and neurotransmitter expression we provide should enhance studies of the CX.

Introduction

The central complex (CX) of the adult *Drosophila melanogaster* brain consists of approximately 2,800 cells that have been divided into 257 cell types based on morphology and connectivity (Scheffer et al., 2020; Hulse et al. 2021; Wolff et al., 2015). These cell types are themselves organized into a set of highly structured neuropils (see Figure 1). The CX plays a key role in the flow of information between sensory inputs and motor outputs. It is particularly important in orientation and navigation, and much progress has been made in defining the cell types and circuits involved in these behaviors (reviewed in Fisher 2022; Green and Maimon 2018; Keram 2022; Turner-Evans and Jayaraman 2016). The CX also appears to participate in sleep and/or activity regulation (reviewed in Dubowy and Sehgal 2017; Shafer and Keene 2021). But these are unlikely to be the only functions performed by the CX.

The connectome has provided a detailed wiring diagram of the CX, information that will be critical for understanding how it performs its functions (Hulse et al., 2021). However, the functions of most cell types in the CX remain unknown. Gaining this knowledge will likely require measuring and manipulating the activity of individual cell types. Such experiments are greatly facilitated by the availability of cell type-specific genetic driver lines. Such lines also allow biochemical approaches for determining the neurotransmitters and neuropeptides used by individual cells. This is particularly relevant for the CX, which is one of the most peptidergic brain areas (Kahsai & Winther, 2011; Nässel and Zandawala, 2019). The roles of neuropeptide signaling in the CX are largely unexplored.

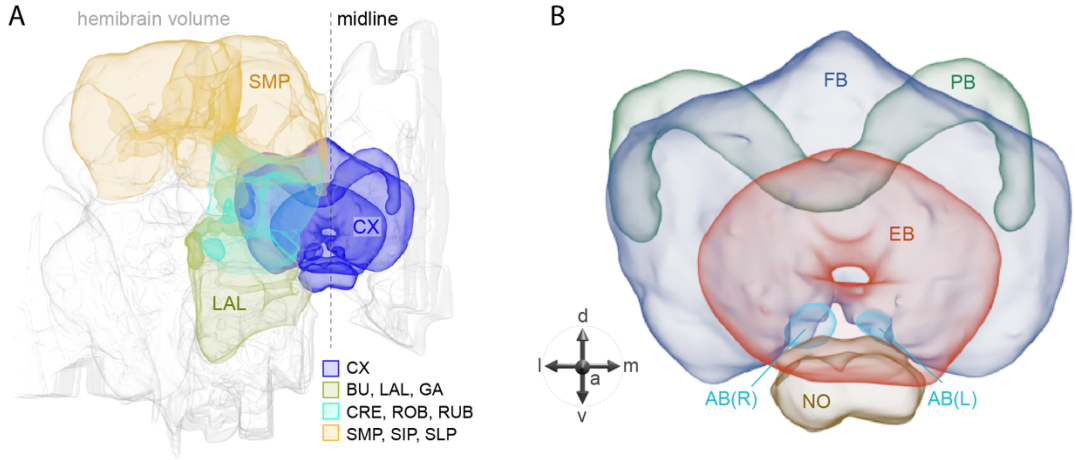

Figure 1. Schematic diagram of CX neuropils. (A) The brain areas included in the hemibrain connectome are shown with the CX and key connected brain areas highlighted. (B) The neuropils comprising the CX are shown: FB, fan-shaped body; PB, protocerebral bridge; EB, ellipsoid body; NO, noduli; and AB, asymmetrical body. Redrawn from Hulse et al. (2021).

In this paper, we present the results of our efforts to develop and characterize genetic driver lines for CX cell types. We also provide a survey of neuropeptide gene expression in the adult central brain as well as determine neurotransmitter (NT) and neuropeptide (NP) gene expression in over 80 CX cell types. Many CX neurons express NPs, with some cell types expressing multiple NPs as well as a fast-acting neurotransmitter. Finally, we demonstrate the use of our collection of driver lines to screen for cell types that influence activity/sleep when activated. In doing so, we uncovered cell types not previously known to play a role in these processes as well as new pathways of communication between the circadian clock and the CX.

Results and Discussion

Generation and analysis of split-GAL4 lines for CX cell types

We generated cell type-specific split-GAL4 lines for CX cell types using the same general approach that we previously applied to the mushroom body (Aso et al., 2014a; Rubin and Aso, 2023) and the visual system (Tuthill et al., 2013; Wu et al., 2016; Nern et al., 2024); see methods for details. In a previous report, we described the generation of split-GAL4 lines for cell types innervating the protocerebral bridge (PB), noduli (NO) and asymmetrical body (AB) (Wolff and Rubin 2018). Here we extend this work to the rest of the CX and include some improved lines for the PB, NO and AB.

Figure 2 and Figure 2—figure supplements 1-4 show the expression of 52 new split-GAL4 lines with strong GAL4 expression that is largely limited to the cell type of interest. All lines were imaged in the brain and ventral nerve cord of adult females, and some were also imaged in males; we did not image expression in the peripheral nervous system or in non-neuronal tissues. Together with the other lines generated in this study and our previous work, we generated high-quality lines for nearly one-third of CX cell types that were defined by analysis of the connectome (Hulse et al., 2021). We also generated lines of lesser quality for other cell types that in total bring overall coverage to more than three-quarters of CX cell types. These additional lines often show some combination of expression in more than one CX cell type, unwanted expression in other brain areas, or weak or stochastic expression. Supplementary File 1 lists the two best split-GAL4 lines we generated for each CX cell type with

comments about their specificity as well as the enhancers used to construct them. Additional split-GAL4 lines used in the sleep and NP/NT studies are also included in this file. Images of all lines are shown at www.janelia.org/split-GAL4 and the original confocal stacks of key imaging data can be downloaded from that site. For a subset of lines, images revealing the morphology of individual cells using MCFO (Nern et al., 2015), and higher resolution images, are also available (see for examples, Figure 3 and Figure 3—figure supplement 1). Additional split-GAL4 lines that may be useful for further studies are listed in Supplementary File 2.

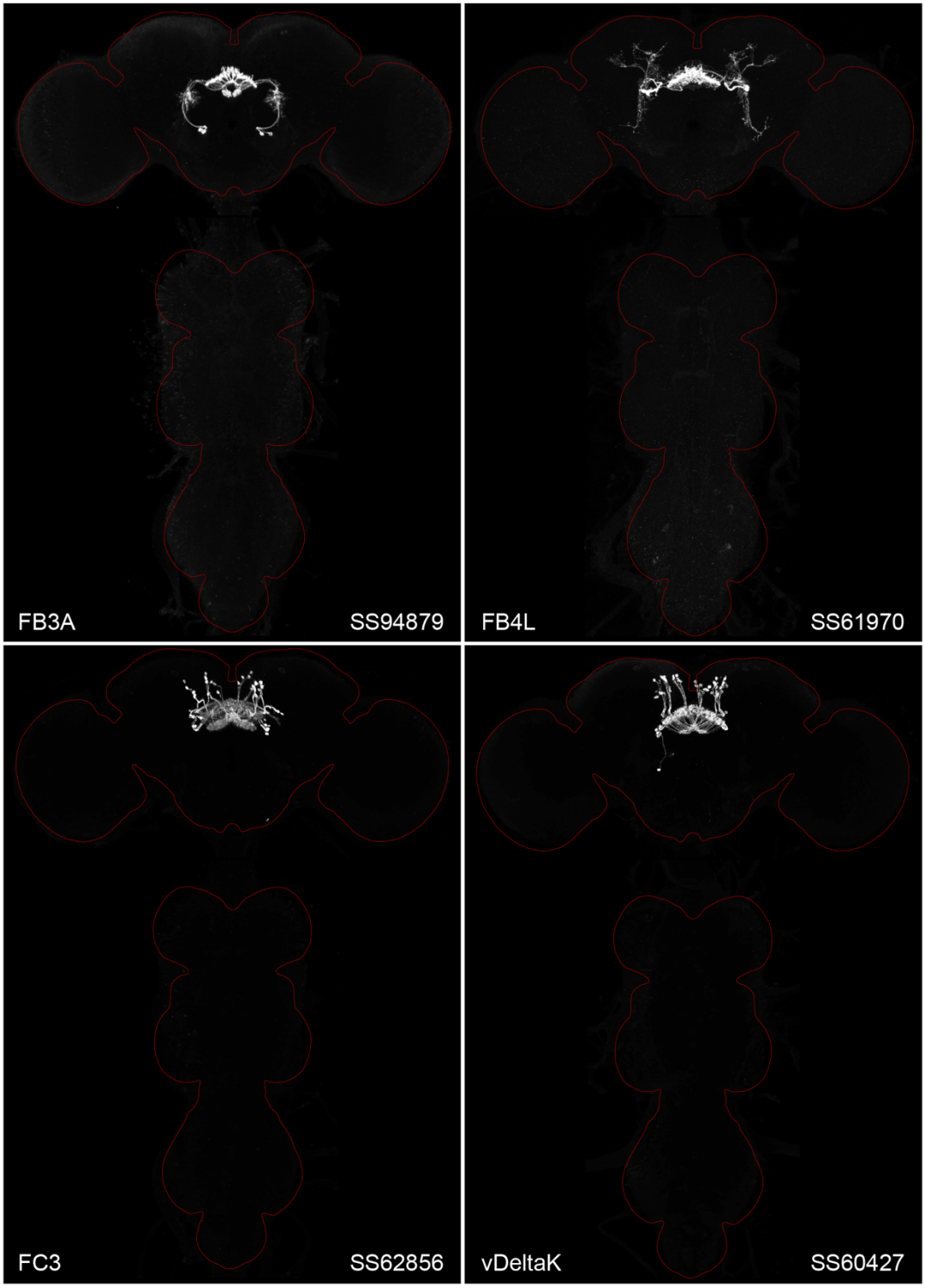

Figure 2. Maximum intensity projections (20X confocal images) of the expression patterns driven by four stable split-GAL4 lines for the indicated cell types. The brain and VNC are outlined in red. Original confocal stacks that include a neuropil reference channel can be downloaded from www.janelia.org/split-gal4. Similar images for 48 additional lines generated as part of this study are shown in Figure 2—figure supplements 1-4.

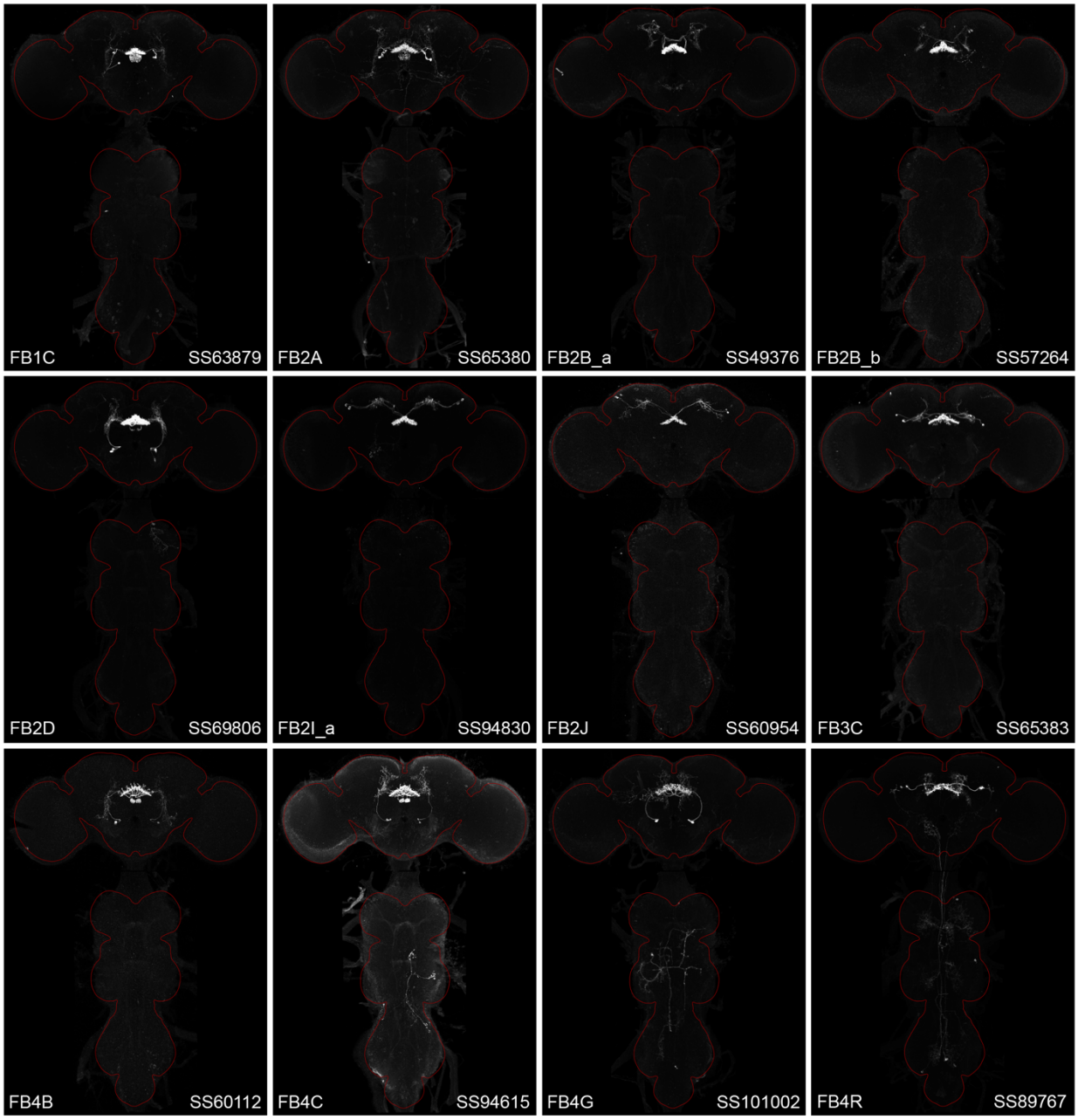

Figure 2—figure supplement 1. Maximum intensity projections (20X confocal images) of the expression patterns driven by stable split-GAL4 lines for the indicated twelve cell types. The brain and VNC are outlined in red. Original confocal stacks that include a neuropil reference channel can be downloaded from www.janelia.org/split-gal4.

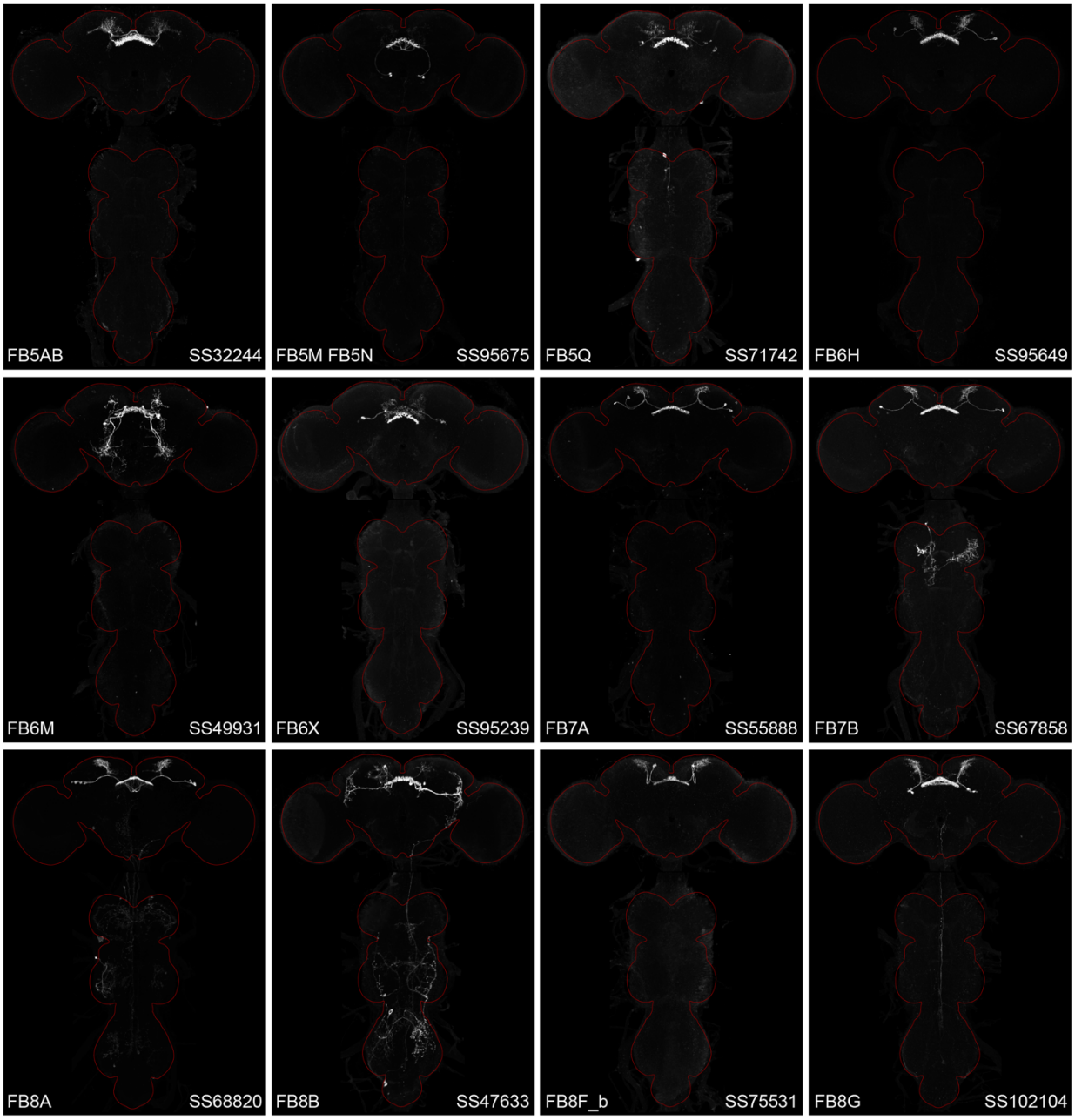

Figure 2—figure supplement 2. Maximum intensity projections (20X confocal images) of the expression patterns driven by stable split-GAL4 lines for the indicated twelve cell types. The brain and VNC are outlined in red. Original confocal stacks that include a neuropil reference channel can be downloaded from www.janelia.org/split-gal4.

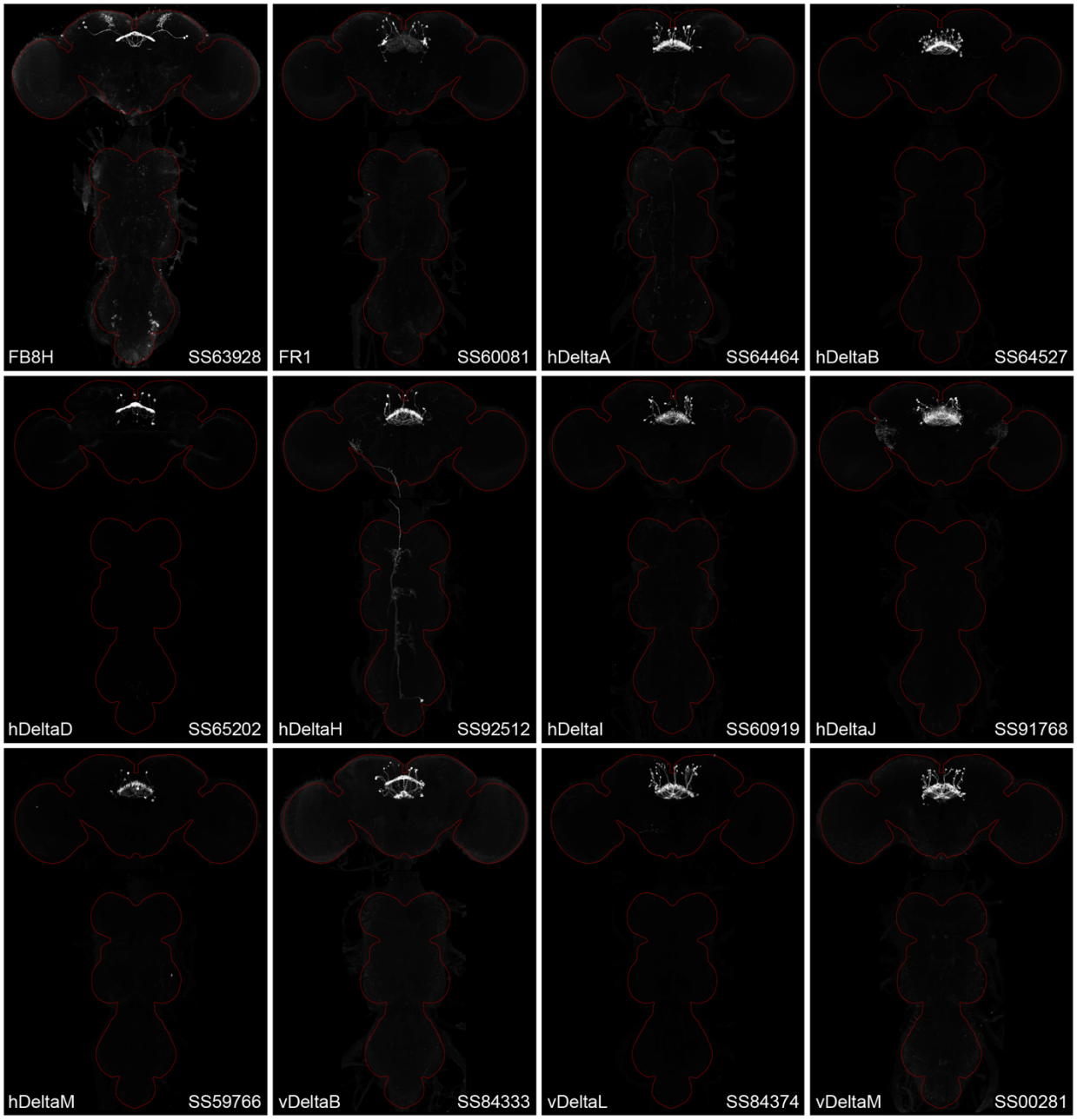

Figure 2—figure supplement 3. Maximum intensity projections (20X confocal images) of the expression patterns driven by stable split-GAL4 lines for the indicated twelve cell types. The brain and VNC are outlined in red. Original confocal stacks that include a neuropil reference channel can be downloaded from www.janelia.org/split-gal4.

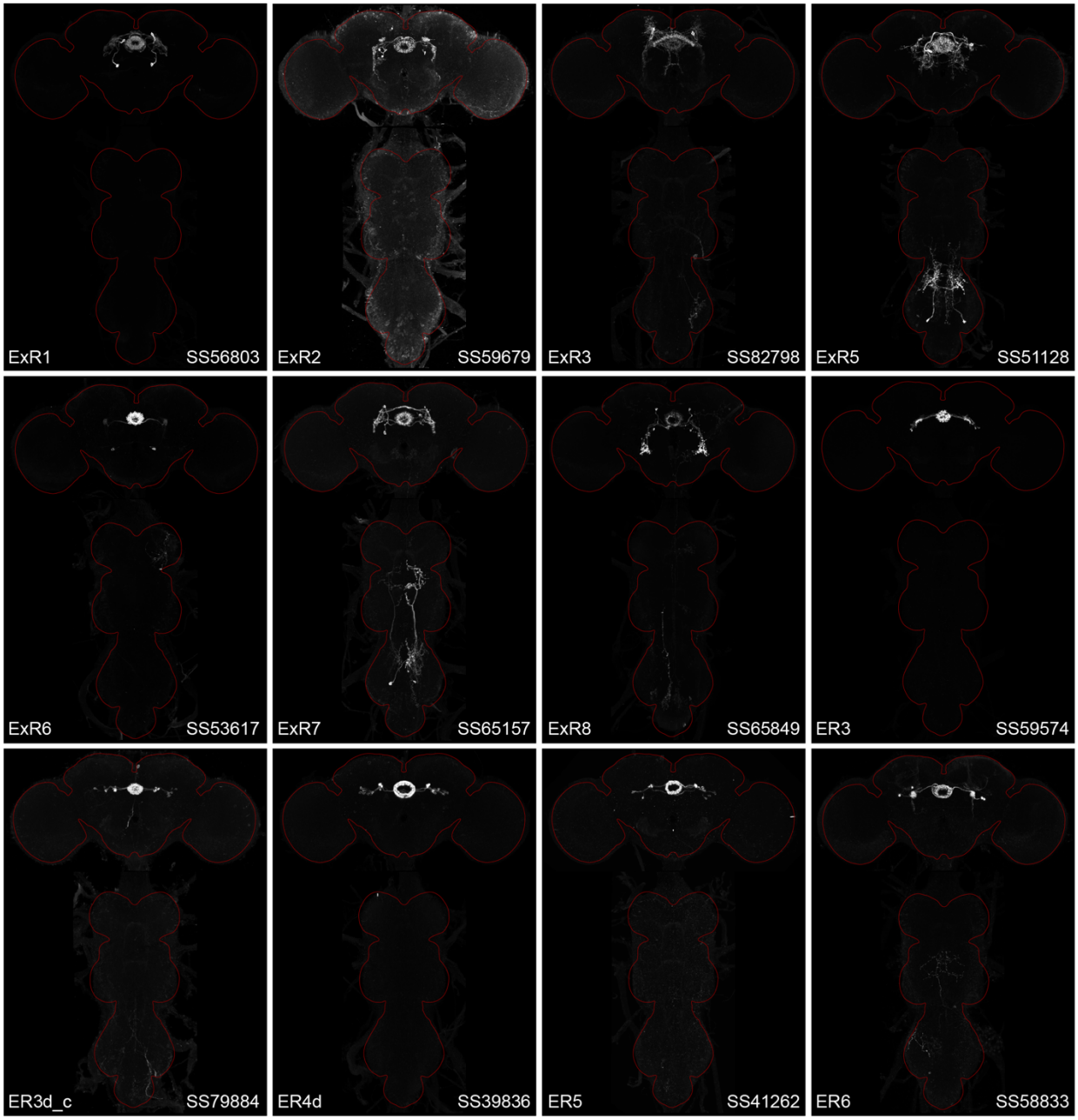

Figure 2—figure supplement 4. Maximum intensity projections (20X confocal images) of the expression patterns driven by stable split-GAL4 lines for the indicated twelve cell types. The brain and VNC are outlined in red. Original confocal stacks that include a neuropil reference channel can be downloaded from www.janelia.org/split-gal4.

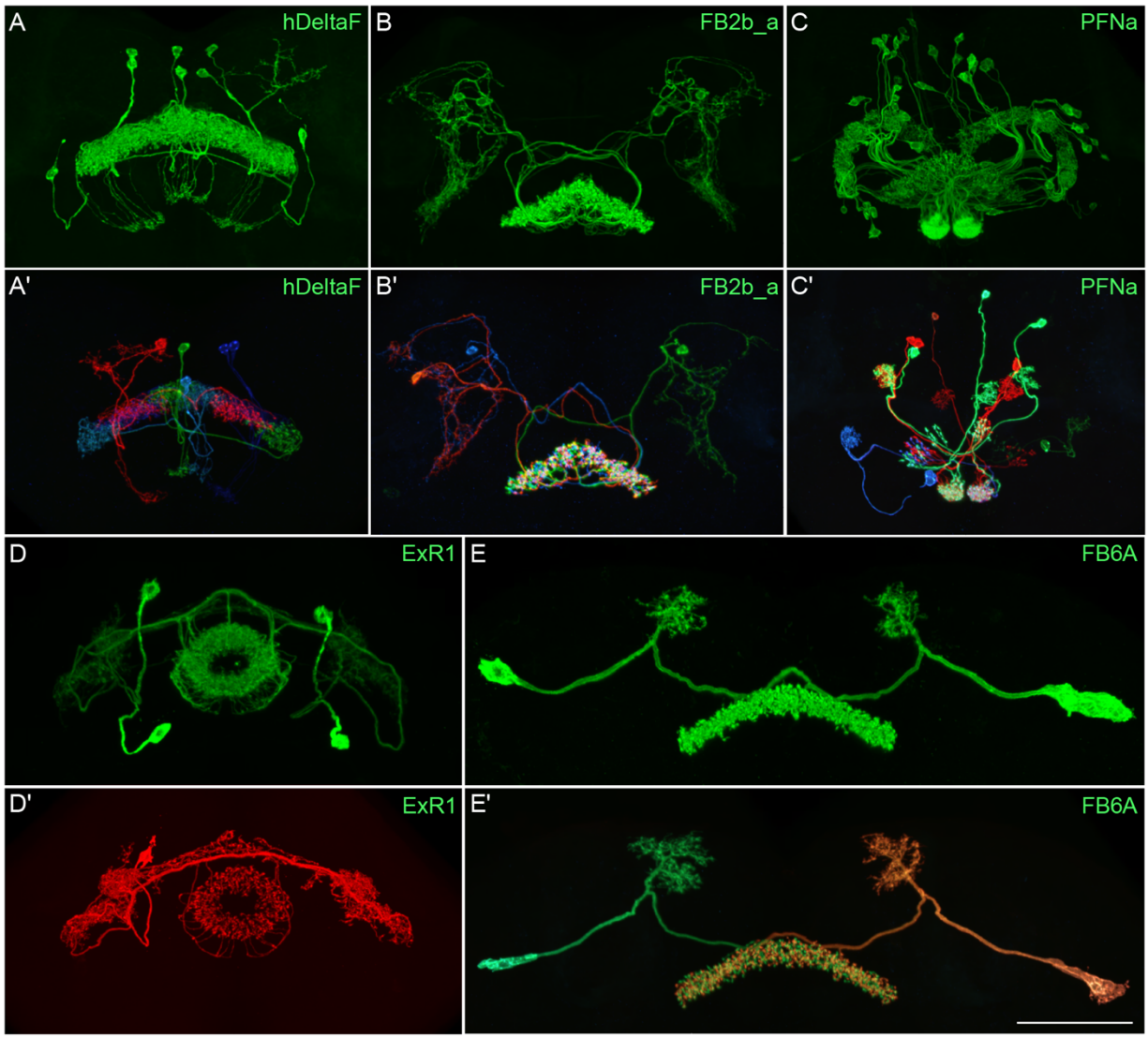

Figure 3. Visualization of the entire expression pattern of a split-GAL4 line for the indicated five cell types revealed using UAS-myrGFP (A-E). A subset of individual cells within those same cell types (A'-E') are revealed by stochastic labeling using the MCFO method (Nern et al. 2015). The scale bar in E' refers to all panels and = 50 μm. Images are maximum intensity projections (MIPs). Stable split lines used were as follows: A, SS54903; A', SS53683; B and B', SS49376; C and C', SS02255; D, SS56684; D', SS56803; E and E', SS57656. The original confocal image stacks from which these images were taken are available at www.janelia.org/split-GAL4.

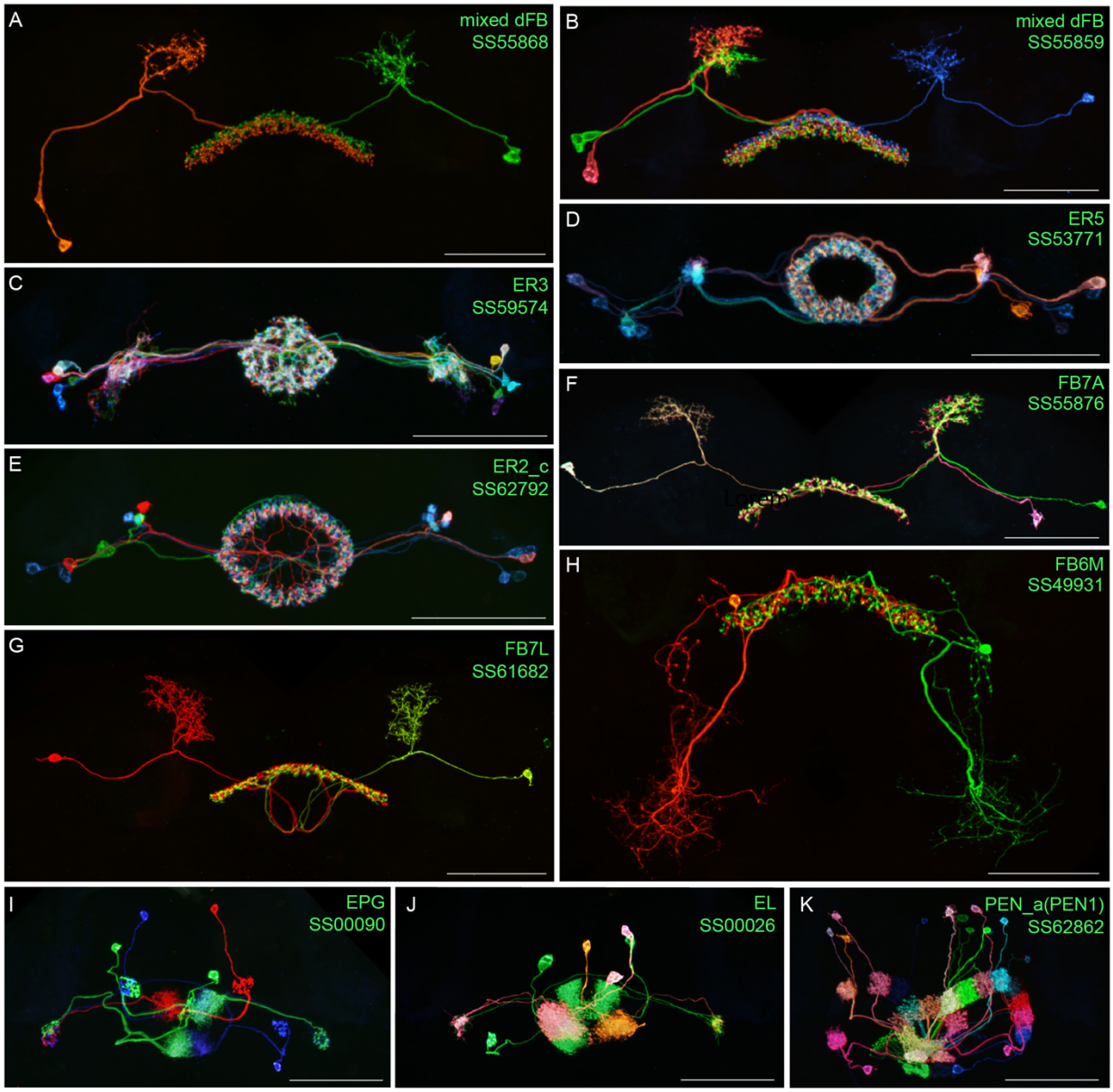

Figure 3—figure supplement 1. Individual cells within the indicated cell types revealed by stochastic labeling using the MCFO method (Nern et al. 2015) with the indicated split-GAL4 lines. Images are MIPs. Scale bars = 50 μm.

Neurotransmitter expression in CX cell types

To determine what neurotransmitters are used by the CX cell types, we carried out fluorescent *in situ* hybridization using EASI-FISH (Close et al., 2024) on brains that also expressed GFP driven from a cell-type-specific split GAL4 line. In this way, we could determine what neurotransmitters were expressed in over 100 different CX cell types based on which members of a panel of diagnostic synthetic enzymes and transporters they expressed: for acetylcholine, ChAT (choline O-acetyltransferase; acetylcholine synthesis) and, in most cases, VAChT (vesicular acetylcholine transporter); for GABA, GAD1 (glutamate decarboxylase; GABA synthesis); for glutamate, vGlut (vesicular glutamate transporter); for dopamine, ple (tyrosine 3-monooxygenase; dopamine synthesis); for serotonin, SerT (serotonin transporter); for octopamine, Tbh (Tyramine β-hydroxylase;

converts tyramine to octopamine); and for tyramine, Tdc2 (Tyrosine decarboxylase 2; converts tyrosine to tyramine) accompanied by lack of Tbh.

Figure 4 shows two examples of this approach. In panels A-D we provide evidence that the PFGs use a less common neurotransmitter, tyramine. Panels E-H show an example of apparent co-transmission. Here, the FB tangential neuron FB4K expresses RNAs suggesting it can release both acetylcholine and glutamate. Cases of co-transmission using two fast acting neurotransmitters have been described in many organisms (reviewed in Svensson et al., 2019) including *Drosophila*, but are rare and may be post-transcriptionally regulated (Chen et al., 2023). Our full results are summarized, together with our analysis of neuropeptide expression in the same cell types, in Figures 5 - 9 and in Supplemental File 1.

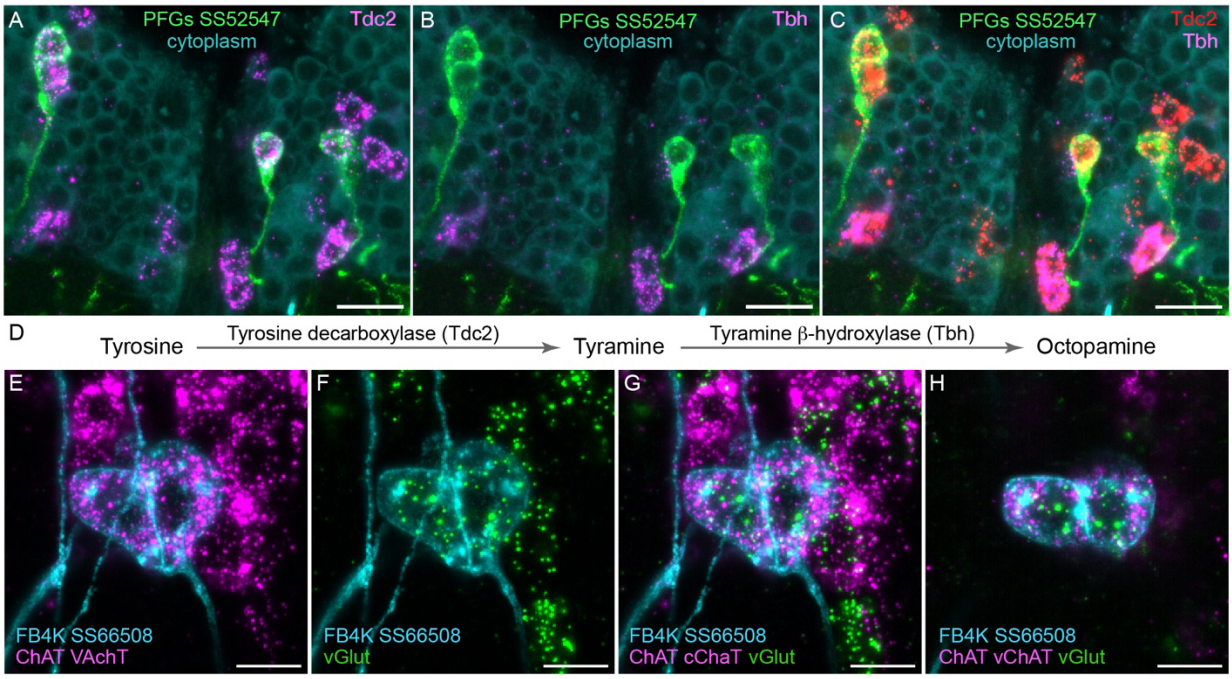

Figure 4. Using EASI-FISH to assess neurotransmitter expression. (A-C) Expression of the transcripts encoding key enzymes required to synthesize tyramine (Tdc2) and octopamine (Tbh) has been examined as indicated. PFG neurons were marked by the split-GAL4 line SS52547 together with UAS-myr-GFP and visualized by anti-GFP antibody staining. Brains were treated with DNAse1 and counterstained with high concentrations of DAPI to reveal total RNA in the cytoplasm. PFG cell bodies show expression of Tdc2 but not Tbh indicating that the PFG neurons use tyramine as a neurotransmitter. Maximum intensity projections (MIPs) of substacks are shown. (D) Biochemical pathway for synthesis of tyramine and octopamine from tyrosine. (E-H) Evidence for co-expression of the neurotransmitters acetylcholine and glutamate in FB4K. EASI-FISH was carried out using probes against choline acetyltransferase (ChAT) and vesicular acetylcholine transporter (VAChT) and vesicular glutamate transporter (vGlut) as indicated. The Fan-shaped body tangential neuron FB4K has been visualized using the split-GAL4 line SS66508. Panels G and H show two different substacks at different Z-depths through the same neurons. Scale bar in each panel = 10 μm.

Methods for using machine learning to predict neurotransmitter from EM images show great promise (Eckstein et al., 2024). However, they are unlikely to fully replace the need for experimental determination and validation for three reasons. First, rarely used transmitters such as tyramine are problematic due to limited training data. Second, accurate prediction of co-transmission is challenging for current computational approaches. Third, FISH remains the gold standard for inferring gene expression.

Survey of neuropeptide and neuropeptide receptor expression in the adult central brain

Neuropeptides provide a parallel mode of communication to wired connections and can act over larger distances using volume transmission (reviewed in Nässel 2009; Bargmann and Marder, 2013). Neuropeptides are widely expressed in the CX (Kahsai et al., 2011; Nässel and Zandawala, 2019) and are likely to play important roles in its function. However, information on the expression of neuropeptides and their receptors is not provided by the connectome. To look for expression of neuropeptides in the CX, we took a curated list of 51 neuropeptide-encoding genes from FlyBase (FB2024_02, released April 23, 2024; Öztürk-Çolak et al., 2024) and eliminated 12 genes based on their not having been detected in RNA profiling studies of the adult brain. Trissin and Natalisin were added to the FlyBase list based on evidence summarized in Nässel and Zandawala (2019). We only examined a small subset of neuropeptide receptors, selecting those whose cognate neuropeptides we thought might play a role in the CX. We used EASI-FISH to determine the expression patterns of these genes in the adult central brain of females (Figures 5-7). The list of 41 neuropeptides and 18 neuropeptide receptors we explored is presented in Figure 5—figure supplement 1.

The neuropeptide expression patterns we observed fell into two broad categories. Some neuropeptides, like those whose expression patterns are shown in Figure 5, appeared to be highly expressed in only a few relatively larger cells. Such large neurosecretory cells often express the transcription factor DIMM (Park et al. 2008). Several of these neuropeptides—for example, SIFa (Terhzaz et al., 2007) and Dsk (Wu et al., 2020)—are expressed in broadly arborizing neurons that appear to deliver them to large areas of the brain and ventral nerve cord. In contrast, neuropeptides like those shown in Figure 6 are expressed in dozens to hundreds of cells and appear poised to function by transmission to nearby cells in multiple distinct circuits. NPF and SIFa appear to act in both these modes. As we show below, most of the neuropeptides shown in Figure 6 are expressed in the CX, each in distinct subsets of cell types.

Neuropeptide receptors (Figure 7) are more broadly, but not uniformly, expressed. In cases where more than one receptor has been identified for a given neuropeptide, such as Dh44 (Figure 7G; reviewed in Lee et al., 2023) and Tk (Figure 7T; see Wohl et al., 2023), the different receptors have distinct, but overlapping, expression pattens.

Neuropeptide expression in CX cell types

We selected 17 neuropeptides whose transcripts were observed in cell bodies located in the same general brain areas as those of the intrinsic cells of the CX (see Figure 5—figure supplement 1). We used probes for these 17 genes to perform EASI-FISH on brains that also expressed GFP in a specific cell type. In this way, we could score neuropeptide expression in individual cell types as we had done for neurotransmitters. Figure 8 shows examples of this approach.

Figure 9 presents a summary table of neurotransmitter and neuropeptide use by individual cell types based on our EASI-FISH results. Supplementary File 1 contains a list of the individual stable split lines that were used for each cell type and how they were scored. We also characterized six CX cell types by RNA profiling (Figure 9—figure supplements 1 and 2) and additional RNA profiling of CX cell types is provided in Epiney et al. (2024). These RNA profiling results are largely congruent with the EASI-FISH data and allow a comparison of transcript number and *in situ* signal strength.

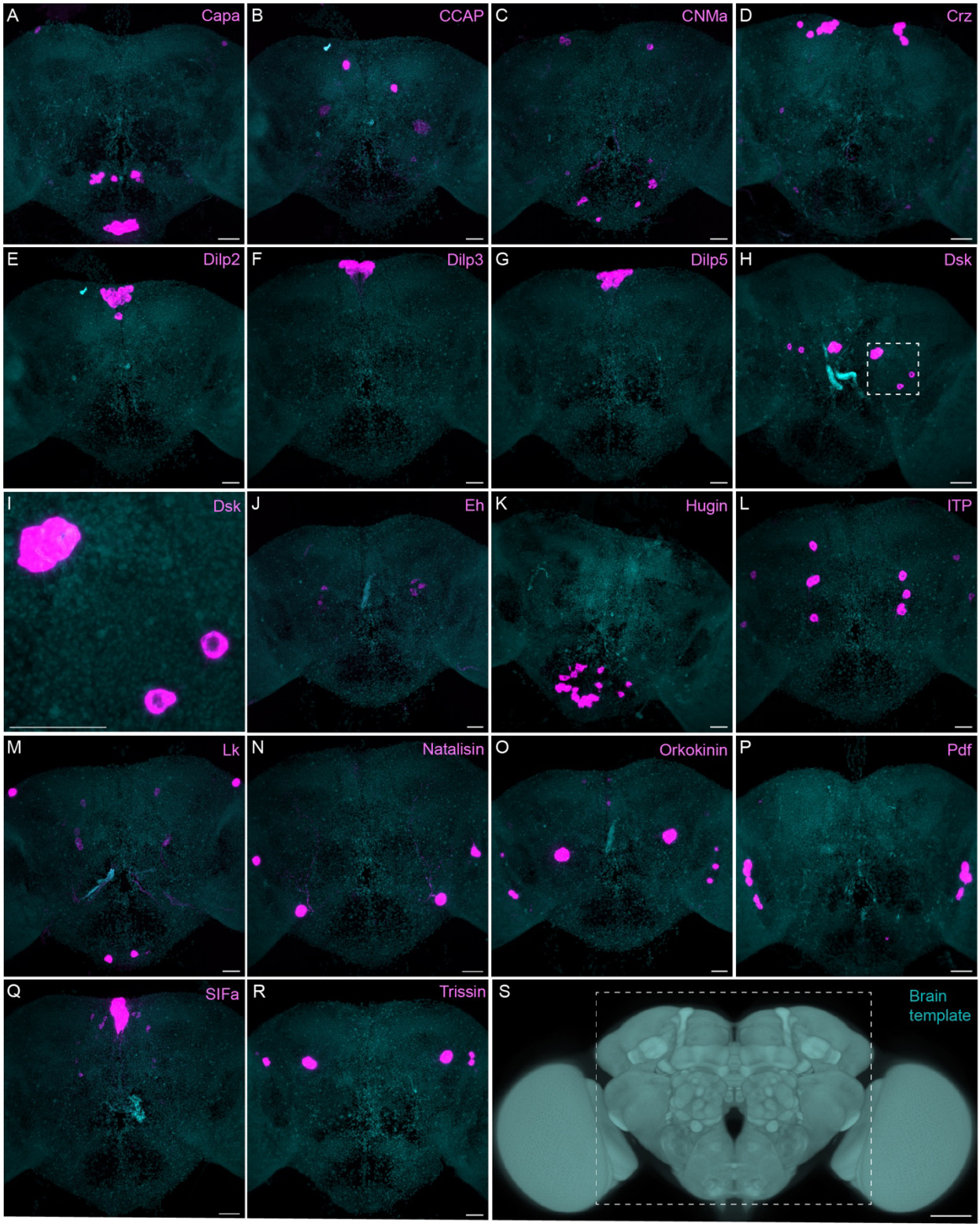

Figure 5. Sparsely expressed neuropeptide genes. EASI-FISH was used to examine the expression of the indicated neuropeptide genes in the central brain (dashed box in S). Samples were counterstained with DAPI to visualize the outline of brain tissue. Images are MIPs. A higher magnification view of a region of the brain showing Dsk expression (indicated by dashed box in H) is shown in I. Scale bar in each panels A-R = 50 μm; note that the images shown are from brains that were expanded by about a factor of two during the EASI-FISH procedure. Scale bar for the unexpanded brain in S = 50 μm.

A few general features emerge from these data. First, more than half of the cell types assayed express a neuropeptide. This frequency is perhaps not surprising given that the CX is considered one of the most peptidergic regions of the adult brain (Kahsai et al., 2011; Nässel and Zandawala, 2019); nevertheless, the fraction of cells expressing an NP appears to be several fold higher in the CX than observed in the adult brain as a whole, as judged by single cell RNA profiling studies (Davies et al., 2018). Second, every cell type that expressed a neuropeptide also expressed a small moleculeneurotransmitter (see Nassel 2018 for a discussion of other cases of co-expression). This co-transmitter was most often acetylcholine or glutamate, but we observed cases of GABA, dopamine, tyramine, octopamine, and serotonin. Third, co-transmission of two small molecule, fast-acting transmitters does occur but is rare. Conversely, co-transmission of a fast-acting transmitter and a modulatory transmitter such as serotonin is common: nine of ten cell types expressing the serotonin transporter also appear to express another small transmitter, most often glutamate or acetylcholine. Octopamine is often, but not always, co-expressed with glutamate (see also Sherer et al., 2020).

Neuropeptides

Symbol	Name	Figures	Notes
Akh	Adipokinetic hormone		negative
amn	amnesiac		negative
AstA	Allatostatin A	6A, 8C	CX candidate
AstC	Allatostatin C	6B, 8D	CX candidate
AstCC	Allatostatin double C		not tested
Burs	Bursicon		not tested
Capa	Capability	5A	
CCAP	Crustacean cardioactive peptide	5B	CX candidate
CCHa1	CCHamide-1	6C	CX candidate
CCHa2	CCHamide-2	6D	CX candidate
CNMa	CNMamide	5C	
Crz	Corazonin	5D	
Dh31	Diuretic hormone 31	6E, 8G, 8N, video 1	CX candidate
Dh44	Diuretic hormone 44	6F, 8P	CX candidate
Dsk	Drosulfakinin	5H, 5I	
Eh	Eclosion hormone	5J	
ETH	Ecdysis triggering hormone		not tested
FMRFa	FMRFamide	6G, 8Q	CX candidate
Gpa2	Glycoprotein hormone alpha 2		not tested
Gpa5	Glycoprotein hormone beta 5		negative
Hug	Hugin	5K	
Ilp1	Insulin-like peptide 1		negative
Ilp2	Insulin-like peptide 2	5E	
Ilp3	Insulin-like peptide 3	5F	
Ilp4	Insulin-like peptide 4		negative
Ilp5	Insulin-like peptide 5	5G	
Ilp6	Insulin-like peptide 6		negative
Ilp7	Insulin-like peptide 7		not tested
Ilp8	Insulin-like peptide 8		not tested
ITP	Ion transport peptide	5L	
Lk	Leucokinin	5M	
Mip	Myoinhibiting peptide precursor	6H, 8F, 8H	CX candidate
Ms	Myosuppressin	6I	CX candidate
Natalisin	Natalisin	5N	
NPF	neuropeptide F	6J, 6K, 8A, 8B	CX candidate
Nplp1	Neuropeptide-like precursor 1	6L, 8R	CX candidate
Nplp2	Neuropeptide-like precursor 2		negative

Neuropeptides (cont.)

Symbol	Name	Figures	Notes
Nplp3	Neuropeptide-like precursor 3		not tested
Nplp4	Neuropeptide-like precursor 4		not tested
Orcokinin	Orcokinin	5O	
Pburs	Partner of Bursicon		not tested
Pdf	Pigment-dispersing factor	5P	
Proc	Proctolin	6M, 8M	CX candidate
Ptth	Prothoracicotropic hormone		not tested
RYa	RYamide		not tested
SIFa	SIFamide	5Q, 8O	CX candidate
sNPF	short neuropeptide F precursor	6N, 8L	CX candidate
SP	Sex Peptide		not tested
spab	space blanket	6O, 8K	CX candidate
Tk	Tachykinin	6P, 8E, 8I, 8J	CX candidate
Trissin	Trissin	5R	

Neuropeptide Receptors

Symbol	Name	Figures
AstA-R1	Allatostatin A receptor 1	7A, 7B
AstC-R1	Allatostatin C receptor 1	7C
CNMaR	CNMamide Receptor	7D, 7E
Dh31-R	Diuretic hormone 31 Receptor	7F
Dh44-R1	Diuretic hormone 44 receptor 1	7G
Dh44-R2	Diuretic hormone 44 receptor 2	7G, video 1
FMRFaR	FMRFamide Receptor	7H
hec	hector	7I
Lgr1	Leucine-rich repeat-containing G protein-coupled receptor 1	7J, 7K
NPFR	Neuropeptide F receptor	7L
Pdfr	Pigment-dispersing factor receptor	7M, 7N, video 1
PK1-R	Pyrokinin 1 receptor	7O
ProcR	Proctolin receptor	7P
SifaR	SIFamide receptor	7Q
sNPF-R	short neuropeptide F receptor	7R
SPR	Sex peptide receptor	7S
TKR86C	Tachykinin-like receptor at 86C	7T
TKR99D	Tachykinin-like receptor at 99D	7T

Figure 5—figure supplement 1. Neuropeptides and neuropeptide receptor genes whose expression patterns were characterized by the EASI-FISH experiments shown in Figures 5-8. Relevant figure panels are listed. Some predicted neuropeptides were not tested because of lack of evidence for their expression in adult brain and are shown in grey font and listed as "not tested" in the Notes column. Neuropeptides shaded in green were tested against split-GAL4 lines with expression in CX cell types (see Figures 8 and 9) based on their cell body positions being in the same brain areas as those of CX cell types. These are listed as "CX candidate" in the Notes column. Those neuropeptides shown in blue font were tested in adult brains, but expression was not detected.; these are listed as "negative" in the Notes column. Lines for which the Notes column is blank were detected in the adult brain but were not chosen for screening against split-GAL4 lines based on the position of their cell bodies.

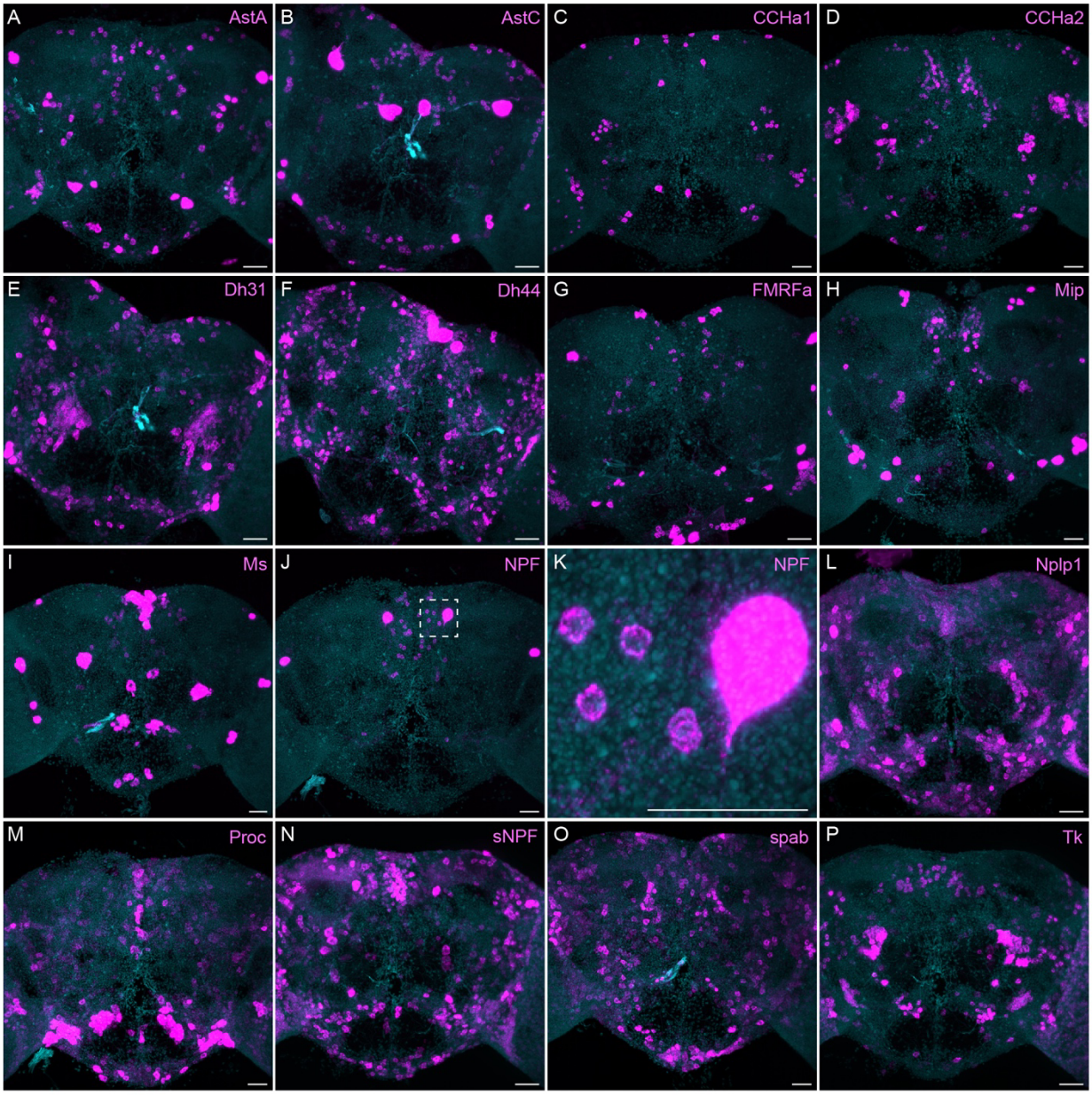

Figure 6. More broadly expressed neuropeptide genes. EASI-FISH was used to examine the expression of the indicated neuropeptide genes in the central brain. Samples were counterstained with DAPI to visualize the outline of brain tissue. Images are MIPs. We included spab and Nplp1 in our screening although it is unclear whether these are indeed neuropeptides (M. Zandawala, pers. comm.). A higher magnification view of a region of the brain showing NPF expression (indicated by dashed box in J) is shown in K. Scale bar in each panel = 50 μm; note that the images shown are from brains that were expanded by about a factor of two during the EASI-FISH procedure.

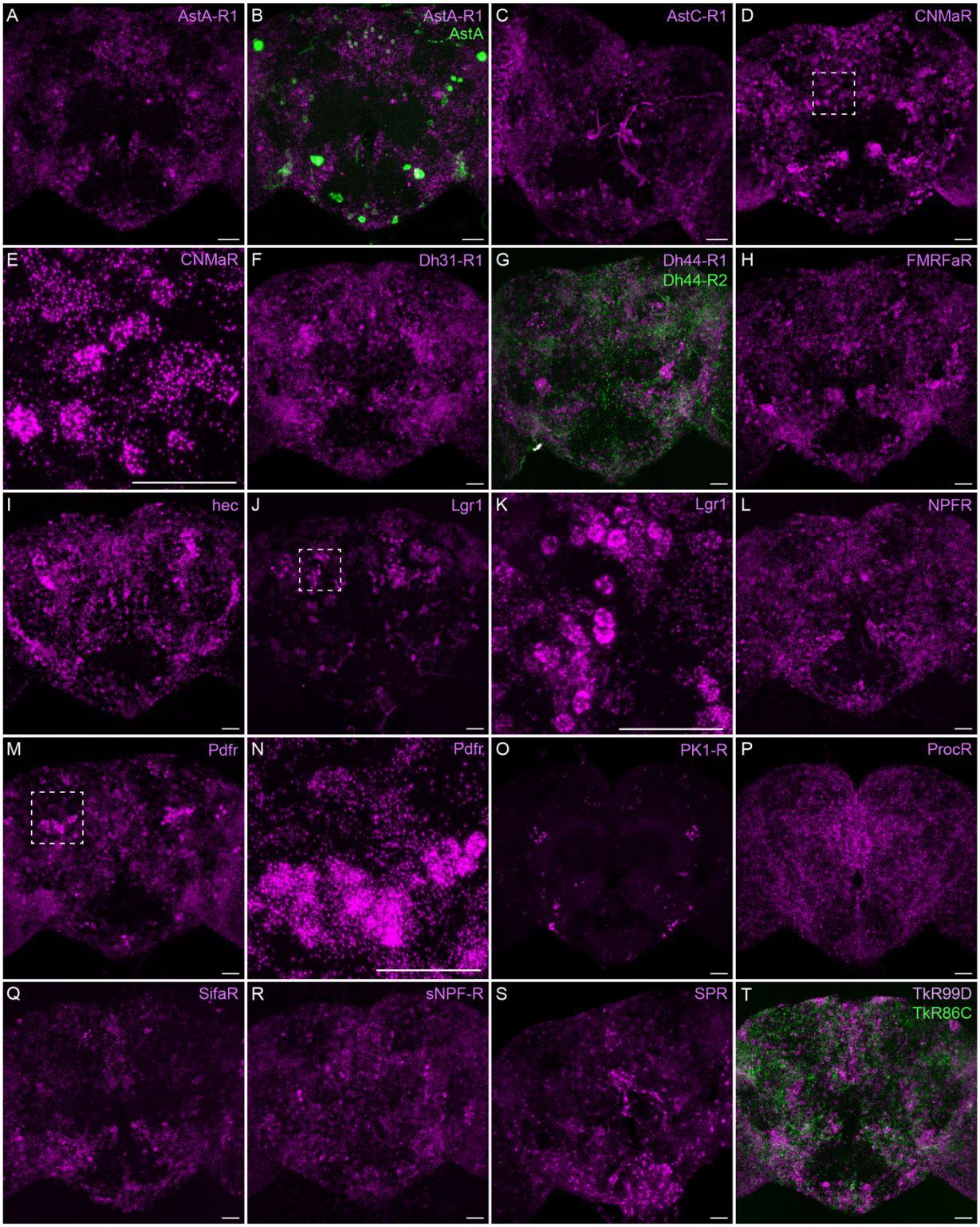

Figure 7. Neuropeptide receptor gene expression. EASI-FISH was used to examine the expression of the indicated neuropeptide genes in the central brain. Higher magnification views of regions of the brains shown in D, J and M (indicated by dashed boxes) are shown in E, K and N. Images are MIPs. Scale bar in each panel = 50 μm; note that the images shown are from brains that were expanded by about a factor of two during the EASI-FISH procedure.

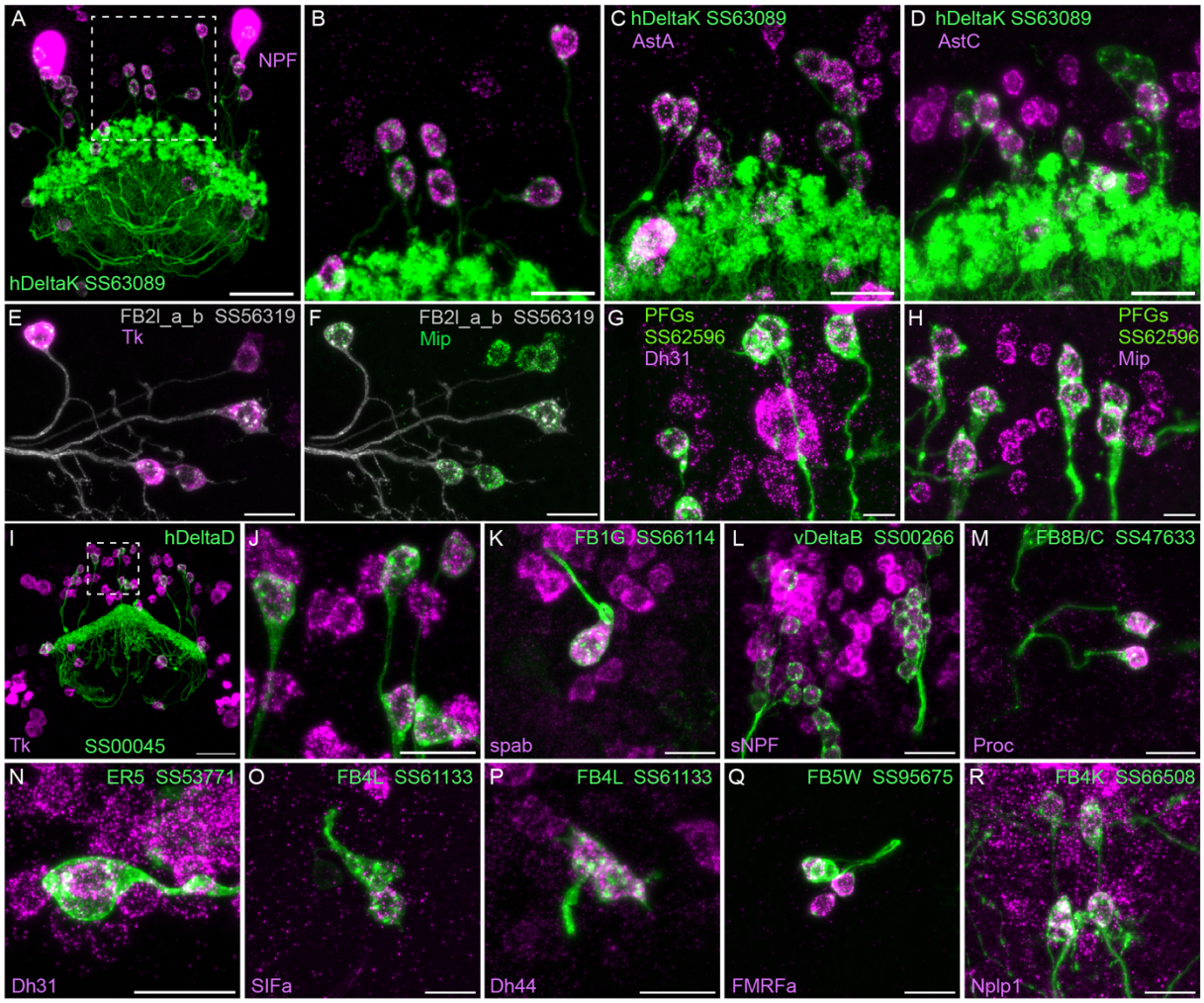

Figure 8. Neuropeptide gene expression in specific cell types. EASI-FISH was used to examine the expression of the indicated neuropeptide genes in the brains also expressing myr-GFP driven by a cell-type-specific split-GAL4 line. The line name and labelled cell type are indicated. GFP was visualized by anti-GFP antibody staining. Hamid et al. (2024) demonstrated expression of Tk in ventral FB neurons likely to correspond to the cell type shown in panel E. Higher magnification view of regions of the brain in A and I (indicated by dashed box) are shown in B and J, respectively. Scale bar in panels A and I = 50 μm and for all other panels = 20 μm; note that the images shown are from brains that were expanded by about a factor of two during the EASI-FISH procedure.

cell type	Neurotransmitters	NT probes	Neuropeptides
PFNp+m	ChAT	1,2,4	**Mip**
PFNd	**ChAT**	1	Dh44
PFNv	*ChAT*	1,2,4	Dh44
PEN_a(PEN1)	*ChAT*	1,2,4	**Dh44, *FMRFa***
PEN_b(PEN2)	**ChAT**	1,2,5	—
PEG	**ChAT**	1,2,4	none detected
EPG	**ChAT**	1	none detected
EPGt	**ChAT**	1	none detected
PFGs	**Tdc2**	1,2,3	**Mip, Dh31**
PFL1	**ChAT**	1,5	—
PFL2	**Tdc2**	1,2,4	**SIFa**
LPsP	**vGlut** **ple** ***SerT***	1,5	—
P6-8P9	**vGlut**	1	—
Delta7	vGlut *SerT*	1,2	***Proc***
P1-9	**vGlut**	1,5	Proc
IbSpsP	**ChAT**	1	—
LNOa	**vGlut**	1	none detected
LCNOpm	**vGlut**	1	—
LCNOp/LCNp	**vGlut**	1	none detected
LNO1	**Gad1**	1	—
vDeltaA_a	ChAT	1,5	—
SA1_b	vGlut	1	—
hDeltaB	**ChAT**	1,5	—
hDeltaC	**ChAT** **SerT**	1,2,3,5	none detected
hDeltaD	ChAT	1,2,3,5	**Dh44, Tk**
hDeltaE	**ChAT**	1,2,3	**Dh44, Tk,** *SIFA*
hDeltaF	**ChAT**	1,2,3	none detected
hDeltaH	**ChAT**	1	**Tk**
hDeltaI	ChAT	1,2,5	AstA
hDeltaK	**ChAT**	1,2,5	**AstA, NPF, *AstC***
hDeltaM	**ChAT**	1	—
vDeltaA_b	**ChAT**	1,5	—
vDeltaB	*ChAT*	1,5	sNPF
vDeltaC	ChAT	1,2,3	**sNPF**, ***Dh31***
vDeltaD	**ChAT**	1,2,3,5	Dh31, **sNPF**
vDeltaE	**ChAT**	1,2,4	Dh31, **sNPF**
vDeltaH	**ChAT**	1	—
vDeltaK	*ChAT*	1,5	—
vDeltaM	ChAT	1,3,5	**Mip**, Dh44

cell type	Neurotransmitters	NT probes	Neuropeptides
FR1	ChAT	1,2,4	**sNPF**
FC1	ChAT	1,2,4	—
FC3	***ChAT*** ***SerT***	1,2,4	—
FB1A	vGlut	1,5	none detected
FB1B	**vGlut**	1,5	none detected
FB1C	*ple*	1,2,5	**Dh44**
FB1D	**vGLuT** ChAT	1,2,4,5	***Mip***
FB1F	**vGlut**	1,5	none detected
FB1G	**ChAT**	1,5	none detected
FB2A	**ple**	1,2,3	—
FB2B_a	vGlut **Tdc2** **SerT**	1,3,5	**Dh44, Proc**
FB2B_b	vGlut **Tdc2** **SerT**	1,3,5	**Dh44, Proc**
FB2C	vGlut	1	none detected
FB2E	**vGlut**	1	**Mip, Tk**
FB2F_a	**vGlut**	1,5	**Dh31**
FB2G_b	**vGlut**	1,5	none detected
FB2H_a	**vGlut**	1	—
FB2H_b	**vGlut**	1	—
FB2I_a	**vGlut**	1,5	**Mip, Tk**
FB2I_b	**vGlut**	1,5	**Mip, Tk**
FB2J	**vGlut**	1	—
FB3A	**vGlut**	1	none detected
FB3C	Gad1	1	**Dh31**
FB3D	vGlut	1,2,3	Dh31
FB4A	**vGlut**	1	Dh31
FB4B	**vGlut**	1	Dh31
FB4C	**vGlut**	1	—
FB4D	**vGlut**	1	none detected
FB4E	vGlut	1	**Dh31**
FB4J	**vGlut**	1	none detected
FB4K	**vGlut** **VAChT**	1	Proc
FB4L	*ple* **Tdc2**	1,2,3	**AstC, Dh44, SIFA**, Ms
FB4M	**ple** ***SerT***	1,2,3	—
FB4N	**vGlut**	1	none detected
FB4O	**vGlut**	1	**Tk**, Dh31
FB4P_b	**vGlut**	1	Dh31, *Tk*
FB4Q_b	vGlut	1	—
FB4R	vGlut	1	**Tk**, Dh31
FB4X	**vGlut**	1	none detected
FB4Y	**SerT**	1,2,3	none detected
FB4Z	**vGlut**	1	Dh44, **Ms**

cell type	Neurotransmitters	NT probes	Neuropeptides
FB5AB	**ChAT**	1	—
FB5B	vGlut	1	none detected
FB5G	vGlut	1	none detected
FB5J	none detected		none detected
FB5K	**vGlut**	1	none detected
FB5L	**vGlut**	1	none detected
FB5N	vGlut	1	**FMRFa**, Proc
FB5Q	vGlut	1	none detected
FB5R	**vGlut**	1	**Dh44**, ***Ms***
FB5T	**vGlut**	1	none detected
FB6A	**vGlut** ChAT	1,5	**AstC**
FB6B	vGlut	1	sNPF
FB6H	**vGLuT** **ple** **SerT**	1,3,5	—
FB6M	**vGlut**	1	**Proc**
FB6P	vGlut	1	—
FB6Q	vGlut	1	—
FB7A	**vGlut**	1,2,3	none detected
FB7B	**vGlut** ChAT **ple** **SerT**	1,5	**Dh31**
FB7G	vGlut	1	—
FB7H	vGlut	1	**Proc**
FB7J	**vGlut**	1	Dh44
FB7L	**vGlut**	1	none detected
FB8B	**vGlut** **Tdc2**	1,2,3,4	**Proc**
FB8C	**vGlut**	1	**Proc**
FB8D	vGlut	1	none detected
FB8F_a	vGlut	1	none detected
FB8F_b	vGlut	1	none detected
FB8H	vGlut	1	none detected
FB9B	**vGlut**	1,2,4	—
EL	**Tdc2** **Tbh**	1,2,3	*SIFa*
ExR1	**ChAT**	1,2,4	none detected
ExR3	**SerT**	1,2,3,4	none detected
ExR5	**vGlut**	1	—
ExR6	**vGlut**	1	—
ExR7	**ChAT**	1	—
ER3d_a	**Gad1**	1	—
ER4m	**Gad1** ple	1,2,4	**Dh31**
ER5	**Gad1**	1,2,4	**Dh31 (PdfR Dh44R2)**
ER6	Gad1	1	—

Expression level	Inputed neurotransmitters
strong expression	ACh, GABA, octopamine, tyramine
weak expression	
very weak expression	Glu, dopamine, seratonin
expression only observed in a subset of GFP-expressing cells	

Figure 9. Summary of neurotransmitter and neuropeptide expression as determined by EASI-FISH performed on adult brains in which selected cell types were marked by a split-GAL4 lines driving GFP expression. About half of all CX cell types were examined using probes for the following 15 NPs: AstA, AstC, CCAP, CCHa1, CCHa2, Dh31, Dh44, FMRFa, Mip, Ms, NPF, Proc, SIFA, sNPF and Tk. All NPs except CCAP, CCHa1, and CCHa2 showed expression in at least one cell type. We excluded spab and Nplp1 from the genes in this Figure, as it is unclear whether these are bonafide neuropeptides (M. Zandawala, pers. comm.); however, data on their expression in the listed cell types is given in Supplemental File 1. See Figures 4 and 8 for examples of the experimental data supporting these conclusions. The specific split-GAL4 driver(s) used for each cell type and other information are given in Supplemental File 1. Results are coded for signal strength by typeface as indicated. The color shading used for neurotransmitters indicates what we believe to be the most likely transmitter used by each cell type. "None detected" indicates that an experiment was performed, whereas a "—" indicates no experimental data. To determine neurotransmitter expression various combinations of probe sets were used as indicated: 1, ChAT and VAChT (choline O-acetyltransferase, and vesicular acetylcholine transporter; GAD1 (glutamate decarboxylase), vGlut (vesicular glutamate transporter); 2, ple (tyrosine 3-monooxygenase), SerT (serotonin transporter), Tbh (Tyramine β hydroxylase); 3, Tdc2 (Tyrosine decarboxylase 2), Tbh; 4, Tdc2; and 5, SerT, ple, Tdc2. In general, all lines were first probed with probe set 1 which reveals expression of genes involved in transmission by acetylcholine (ChAT), GABA (GAD) and glutamate (vGlut). Then a subset of lines was probed for genes involved in transmission by dopamine (ple), serotonin (SerT), octopamine (Tbh and Tdc2) and tyramine (Tdc2).

Neurotransmitters

Gene	ER5	ExR1	hDeltaK	FB6A	FB6A	FB7A	FB2
	Cell Type						
ChAT	7.51	10.05	10.81	6.95	7.83	8.20	8.70
VAChT	6.06	8.66	8.63	5.40	5.83	6.71	6.15
VGlut	5.64	3.46	5.25	8.99	8.75	9.47	9.16
Gad1	10.60	4.80	6.38	3.46	4.46	5.23	4.76
VGAT	7.95	4.25	5.68	3.55	3.10	4.27	4.92
ple	0.00	0.26	0.00	3.73	4.02	0.00	-1.17
Ddc	9.09	7.70	10.75	7.93	6.51	8.43	9.53
DAT	2.22	4.00	0.00	8.50	7.16	7.81	3.04
Vmat	0.00	3.66	4.71	9.81	4.73	1.81	8.05
Trh	1.87	1.77	4.02	6.24	6.72	8.55	6.32
SerT	0.00	-0.74	0.00	-0.42	-1.32	-1.00	5.07
Tbh	8.46	1.26	6.96	6.83	3.14	4.15	5.91
Tdc1	0.00	0.00	-2.32	-2.00	1.93	-2.00	0.00
Tdc2	0.00	-0.32	-0.74	4.29	-2.32	-2.00	0.00
prt	6.08	0.49	7.79	6.10	2.26	4.36	5.68

Neurotransmitter Receptors

Gene	ER5	ExR1	hDeltaK	FB6A	FB6A	FB7A	FB2
	Cell Type						
mAChR-A	9.42	7.91	7.79	5.29	5.69	7.95	8.08
mAChR-B	3.32	1.49	0.00	3.52	4.07	7.54	2.42
mAChR-C	0.00	0.00	0.00	0.00	0.00	0.00	0.00
nAChRalpha1	6.87	6.54	6.77	4.74	4.05	5.24	5.11
nAChRalpha2	5.38	5.97	4.60	0.58	5.15	5.63	5.53
nAChRalpha3	6.14	9.06	6.08	6.88	6.04	6.25	7.66
nAChRalpha4	6.31	6.00	7.25	4.43	4.51	5.06	5.42
nAChRalpha5	9.70	7.54	9.07	7.92	6.66	8.31	8.34
nAChRalpha6	12.55	7.75	10.99	9.37	9.70	10.13	9.84
nAChRalpha7	11.94	7.71	9.04	7.69	6.20	6.79	7.31
nAChRbeta1	9.77	10.50	9.66	8.55	8.46	9.04	10.33
nAChRbeta2	7.74	6.41	7.10	5.55	5.68	6.44	7.14
nAChRbeta3	0.00	0.00	0.00	-2.00	-2.32	0.00	0.00
GABA-B-R1	4.32	7.77	7.44	6.41	6.31	6.32	6.71
GABA-B-R2	6.60	6.50	7.05	5.52	4.41	7.20	6.27
GABA-B-R3	4.00	3.83	3.51	1.00	0.26	4.44	5.68
Rdl	12.88	12.14	11.15	10.27	10.28	10.82	11.82
Lcch3	6.38	6.08	6.12	5.54	4.12	3.93	6.07

-3.0 9.0 14

Neurotransmitter Receptors

Gene	ER5	ExR1	hDeltaK	FB6A	FB6A	FB7A	FB2
	Cell Type						
GluRIA	2.94	5.53	6.51	8.29	8.04	6.87	4.81
GluRIIA	-1.58	0.85	0.00	1.17	0.00	0.00	0.00
GluRIB	4.68	7.58	6.04	9.15	8.70	7.40	4.66
GluRIIB	0.00	0.00	-2.32	0.00	0.00	-2.00	-0.85
GluRIIC	0.00	-2.32	-2.32	0.00	1.26	0.00	-1.58
GluRIID	0.00	0.00	0.00	-2.00	2.63	0.00	0.00
GluRIIE	0.00	0.00	-2.32	-2.00	-0.74	0.00	0.00
mGluR	5.68	1.00	4.38	5.04	1.49	4.19	4.98
dmGlut	0.00	0.00	0.00	1.32	-0.74	0.00	-2.17
GluClalpha	6.07	10.14	7.88	7.09	7.01	7.50	7.98
CG11155	8.64	7.48	7.93	6.82	6.78	8.16	8.13
KaiR1D	6.65	4.66	5.78	4.70	3.81	6.29	6.07
Ekar	0.00	-0.74	1.77	0.32	1.38	3.46	-0.36
clumsy	0.00	2.38	0.00	-2.00	-0.32	0.00	-3.17
Grik	4.20	3.23	4.02	3.49	-1.32	3.32	-0.85
Nmdar1	3.81	4.64	1.00	3.75	2.93	6.30	5.46
Nmdar2	7.68	7.49	6.14	6.13	6.01	5.68	5.45
GlyT	5.39	6.92	5.93	5.33	4.15	3.64	6.43
Grd	0.00	-2.32	1.68	2.81	5.28	6.67	2.22
SecCl	0.00	4.41	0.00	-0.42	-2.32	0.00	0.00
CG12344	0.00	0.00	0.00	0.58	-0.32	3.73	-2.17
Hdc	0.00	-0.74	0.00	0.00	-0.32	0.00	-2.17
ort	-1.58	-0.74	0.00	1.46	1.68	0.00	2.04
HisCl1	0.00	-0.74	0.00	-2.00	-0.32	0.00	-3.17
Dop1R1	3.97	6.38	6.87	8.39	9.04	7.74	6.64
Dop1R2	3.84	5.60	2.43	4.43	5.05	5.61	7.29
Dop2R	6.74	8.48	9.32	9.63	7.86	9.53	9.15
DopEcR	8.04	8.04	6.95	7.33	6.58	5.78	7.26
Oamb	9.92	3.87	5.66	3.17	3.68	3.88	4.12
Octbeta1R	4.72	6.84	5.42	9.85	9.20	10.46	4.77
Octbeta2R	2.58	5.09	7.46	3.64	4.72	3.29	3.61
Octbeta3R	3.77	5.50	5.19	6.40	6.89	7.71	4.70
Oct-TyrR	5.47	6.33	0.85	1.91	0.26	0.58	5.79
TyrR	1.00	1.14	0.49	3.09	1.26	0.58	1.69
TyrRII	0.00	-2.32	0.00	0.32	-2.32	1.70	0.00
5-HT1A	6.70	5.94	5.15	5.14	2.32	4.44	7.41
5-HT1B	-1.58	4.78	1.49	2.58	4.70	-2.00	4.93
5-HT2A	8.48	2.93	4.34	7.92	7.11	7.26	3.98
5-HT2B	0.00	4.43	8.22	6.78	5.60	-0.42	3.02
5-HT7	6.00	3.17	5.49	5.99	4.70	4.51	0.74

Figure 9—figure supplement 1. RNA-seq data for genes related to neurotransmitter synthesis, transport, and receptors in the indicated cell types. Mean $\log_2$ of TPM values for each gene are listed. See NCBI Gene Expression Omnibus (accession number GSE271123) for the raw data. The split-GAL4 drivers used for each cell type were as follows: ER5, SS00070; ExR1, SS56684; hDeltaK, SS02748; FB6A, SS57656 and SS54343; FB7A, SS55888; FB2, SS56319.

Neuropeptides

Gene	ER5	ExR1	hDeltaK	FB6A	FB6A	FB7A	FB2
	Cell Type						
Akh	0.00	0.85	0.00	-2.00	2.07	2.25	2.26
amn	1.58	-1.32	4.14	0.00	0.00	-0.42	1.08
AstA	1.22	0.49	13.49	1.32	-2.32	0.00	-3.17
AstC	5.55	0.49	6.94	8.51	12.28	5.02	-1.58
Burs	0.00	0.00	0.00	0.00	0.00	0.00	0.00
Capa	0.00	-0.74	-0.32	0.00	0.00	0.00	0.00
CCAP	0.00	0.00	0.00	0.00	-0.74	-1.00	0.00
CCHa1	0.00	-0.32	0.00	0.00	-2.32	0.00	-1.58
CCHa2	0.00	0.68	1.58	2.70	-0.74	0.00	2.32
CNMa	0.00	-1.32	0.00	-2.00	0.00	-2.00	0.00
Crz	0.00	0.00	-0.74	0.00	-2.32	0.00	6.63
Dh31	12.77	3.77	7.85	0.00	3.94	0.00	4.81
Dh44	2.74	4.70	5.98	5.33	1.26	0.00	1.64
Dsk	0.00	0.00	0.00	0.00	-1.32	0.00	0.00
Eh	0.00	0.00	0.00	-2.00	2.07	0.00	0.00
ETH	0.00	0.00	0.00	0.00	2.58	0.00	1.87
FMRFa	0.00	-0.74	-2.32	0.00	0.00	-2.00	0.92
Hug	0.00	0.00	0.00	0.00	0.26	0.00	1.35
ITP	0.00	4.32	3.41	2.09	0.26	0.00	-0.17
Lk	0.00	-2.32	0.00	0.00	0.00	0.00	0.00
Mip	5.32	1.58	0.00	5.39	5.37	5.86	12.94
Ms	0.00	3.35	0.00	3.93	1.00	-1.00	3.15
NPF	0.00	-2.32	12.02	0.00	-2.32	0.00	-3.17
Nplp1	8.05	4.07	4.57	7.68	5.86	9.17	8.34
Nplp3	0.00	0.00	-2.32	0.00	0.00	0.00	0.00
Nplp4	0.00	0.00	0.00	0.00	1.38	0.00	0.00
Orcokinin	0.00	0.00	0.00	0.00	-1.32	3.98	3.58
Pburs	0.00	0.00	0.00	0.00	-2.32	0.00	0.00
Pdf	0.00	-2.32	0.00	0.00	-0.74	-2.00	0.42
Proc	4.39	4.63	8.69	3.17	-0.32	0.81	2.12
Ptth	0.00	0.00	0.00	0.00	0.00	0.00	-3.17
RYa	0.74	0.00	-1.32	6.46	6.06	9.07	5.90
SIFa	0.00	0.00	0.00	0.00	-2.32	0.00	0.00
sNPF	5.40	5.31	6.64	4.02	3.72	3.39	3.27
Tk	0.00	3.93	4.22	4.92	2.89	5.13	13.63
Trissin	0.00	1.68	-2.32	0.00	-1.32	0.00	1.08

-3.0 9.0 14

Neuropeptide Receptors

Gene	ER5	ExR1	hDeltaK	FB6A	FB6A	FB7A	FB2
	Cell Type						
AkhR	0.00	-1.32	3.41	0.00	-1.32	0.00	-1.17
AstA-R1	-1.58	2.07	9.23	6.60	4.95	8.06	4.31
AstA-R2	0.00	4.89	0.00	0.58	4.62	0.00	0.00
AstC-R1	5.00	0.68	0.85	2.46	-0.74	-1.00	2.71
AstC-R2	4.27	6.50	1.14	1.70	2.58	-0.42	0.00
CapaR	0.00	0.00	0.00	-0.42	-2.32	0.00	-1.58
CCAP-R	0.00	-0.32	-2.32	0.00	-0.32	0.00	5.85
CCHa1-R	0.00	1.68	1.38	0.00	0.00	0.00	4.60
CCHa2-R	0.00	-1.32	-1.32	0.00	0.00	-2.00	2.50
CCKLR-17D1	0.00	-0.74	3.96	1.17	-2.32	0.00	-0.36
CCKLR-17D3	0.00	1.58	4.52	2.70	2.54	3.04	1.15
CG10738	-1.58	-0.32	1.49	0.58	3.29	4.81	4.10
CG13229	0.00	3.23	4.47	-0.42	4.36	2.81	3.27
CG13575	0.00	0.00	-2.32	0.00	0.00	0.00	0.00
CG13579	0.00	0.00	0.00	2.70	-0.32	5.99	2.96
CG13995	7.67	6.51	7.86	4.95	5.28	5.70	6.45
CG30340	-1.58	-0.32	0.00	1.81	-2.32	-2.00	-3.17
CG32547	6.55	5.97	5.26	3.55	-1.32	-2.00	0.92
CG33639	2.94	5.41	7.85	4.48	3.94	3.75	6.30
CNMaR	-1.58	6.26	7.94	5.61	3.41	3.75	10.69
CrzR	2.00	2.54	0.00	0.32	-1.32	3.88	-1.17
Dh31-R	6.31	3.66	3.54	0.00	-0.32	0.00	4.88
Dh44-R1	3.58	7.10	2.32	3.61	1.85	4.91	4.12
Dh44-R2	7.16	5.29	5.39	2.09	3.29	4.11	2.98
ETHR	6.04	4.29	3.61	4.04	5.07	2.91	4.91
FMRFaR	0.00	6.45	3.43	3.88	2.49	0.32	-0.58
hec	0.00	1.14	1.00	6.07	5.41	8.01	7.28
Lgr1	0.00	1.58	0.49	0.00	0.00	5.48	7.07
Lgr3	3.00	0.49	0.00	-0.42	-0.74	3.39	1.69
Lgr4	0.00	0.68	1.85	1.58	-0.32	2.00	-0.85
Lkr	0.00	-2.32	0.00	-1.00	-0.32	0.00	0.42
MsR1	0.00	3.20	3.87	-0.42	-0.32	5.12	3.53
MsR2	0.00	1.68	2.93	1.81	-2.32	3.21	-0.85
NPFR	0.00	1.49	6.69	0.00	2.38	6.09	5.15
Pdfr	9.92	5.72	4.00	1.70	3.51	0.58	7.27
PK1-R	0.00	0.26	0.00	-2.00	-1.32	0.00	0.00
PK2-R1	0.00	5.51	-2.32	0.00	-0.74	0.00	1.47
PK2-R2	2.66	4.60	1.38	-2.00	-1.32	0.00	2.47
Proc-R	1.22	0.00	3.20	0.00	-2.32	0.00	2.58
rk	-1.58	3.00	3.74	-1.00	-0.32	-1.00	3.13
RYa-R	3.06	0.00	0.00	1.70	-1.32	3.00	-0.58
SIFaR	0.00	6.07	6.00	6.63	3.72	-1.00	4.97
sNPF-R	5.00	6.42	0.00	2.00	-0.74	0.00	4.03
TkR86C	4.32	0.49	0.00	1.70	0.00	0.00	4.43
TkR99D	6.75	0.00	0.00	-2.00	0.00	4.13	6.35
TrissinR	2.00	4.50	2.32	1.00	2.89	0.00	2.53

Figure 9—figure supplement 2. RNA-seq data for genes related to neuropeptides and their receptors in the indicated cell types.

Screen for cell types whose activation modifies sleep

Sleep is a behavior widely studied in *Drosophila* (reviewed in Dubowy and Sehgal 2017; Shafer and Keene 2021). The phenotypic description of sleep and its relationship to activity, as well as the cell types that play a role in sleep regulation are under active study in many labs. The CX has been documented to be a significant brain region for sleep regulation. But many cell types in the CX have never been assayed for a role in sleep due to the lack of suitable genetic reagents. Therefore, we used our genetic drivers for CX cell types to screen for those whose activation by thermogenetics or optogenetics strongly influenced sleep or activity. As described in methods, we used three metrics: sleep duration; P(Doze), the probability that an active fly will stop moving; and P(Wake), the probability that a stationary fly will start moving. These assays were carried out over several years in parallel with our building the collection of lines, so many of the lines we assayed did not make it into our final collection of selected lines. Conversely, we did not assay all our best lines as many only became available after our behavior experiments were completed.

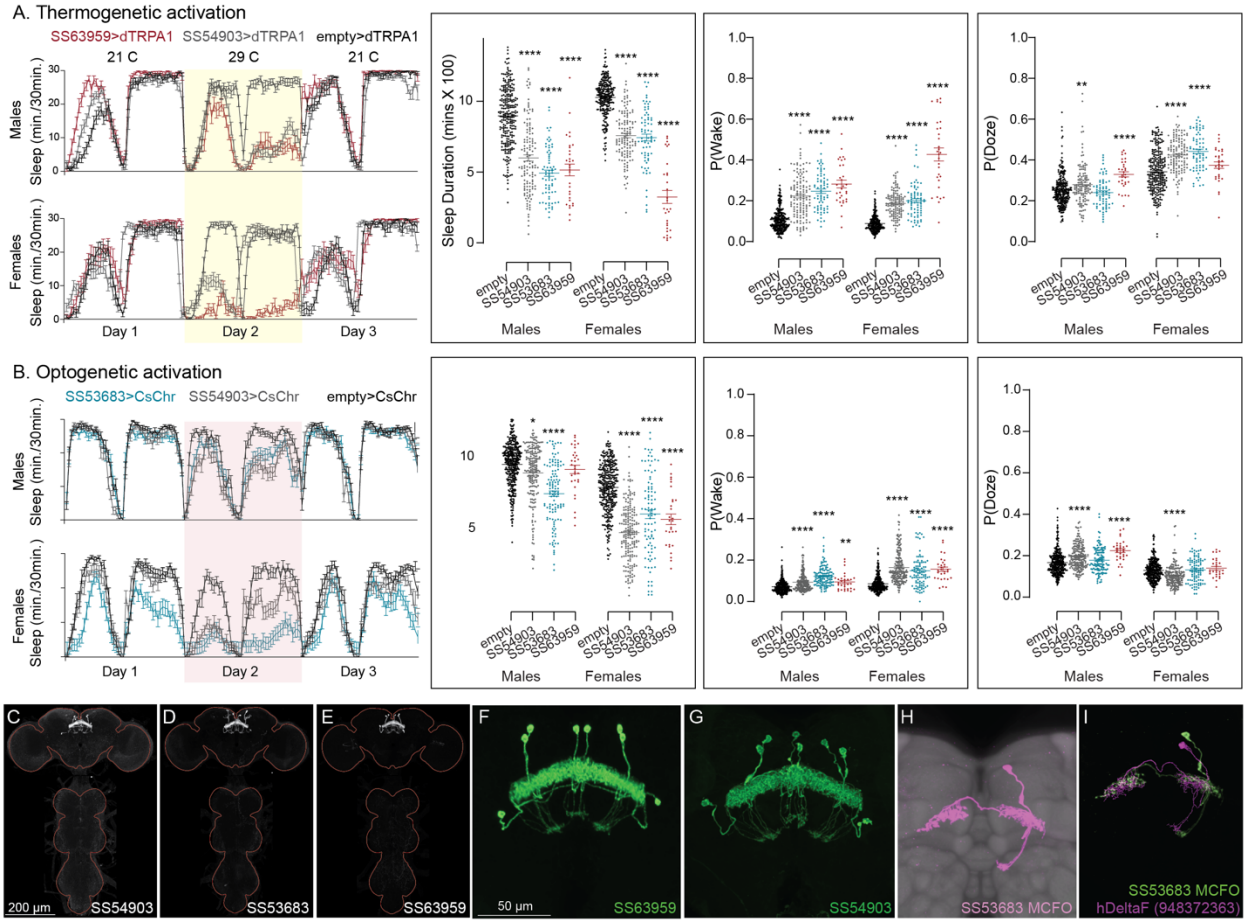

Figure 10. Activation of hDeltaF, comprised of eight intrinsic FB columnar neurons (see Hulse et al., 2021) decreases sleep. (A) Thermogenetic activation and DAM based monitoring using the split-GAL4 lines SS54903, SS53683 and SS63959 produced decreased sleep duration and increased P(Wake) in all three lines as compared to the control (empty-GAL4). The sleep profile indicated a stronger suppression of sleep during nighttime in males and reduced sleep during both day and nighttime in females. (B) Optogenetic activation and video-based tracking showed that two split-GAL4 lines (SS54903 and SS53683) have decreased sleep duration, and all three tested lines have increased P(Wake) in male flies during optogenetic activation. All three lines showed decreased sleep and increased P(Wake) in female flies. As observed with thermogenetic activation, these phenotypes were more pronounced for nighttime sleep in males. In addition to sleep duration and P(Wake) we also measured activity by beam counts/waking minute in the DAM assays and pixel movements/waking minute in video tracking. We found that activation of hDeltaF does not increase these measures, showing that observed changes are not attributable to hyperactivity (see Supplementary Files 3-6). (C-E) MIP images of GFP-driven expression in the brain and VNC of the three spilt-GAL4 lines. The brain and VNC are outlined in red. (F,G) Higher resolution images of the relevant brain area of two of the lines. (H) Morphology of a single neuron revealed by stochastic labelling. (I) Comparison of LM and EM cell morphologies. Original confocal stacks for panels C-H can be downloaded from www.janelia.org/split-gal4. The full genotypes of the driver lines are given there and in Supplementary File 1. Statistical comparisons were made by Kruskal-Wallis and Dunn's post hoc test. Asterisk indicates significance from 0: *p<0.05; **p<0.01; ****p<0.0001.

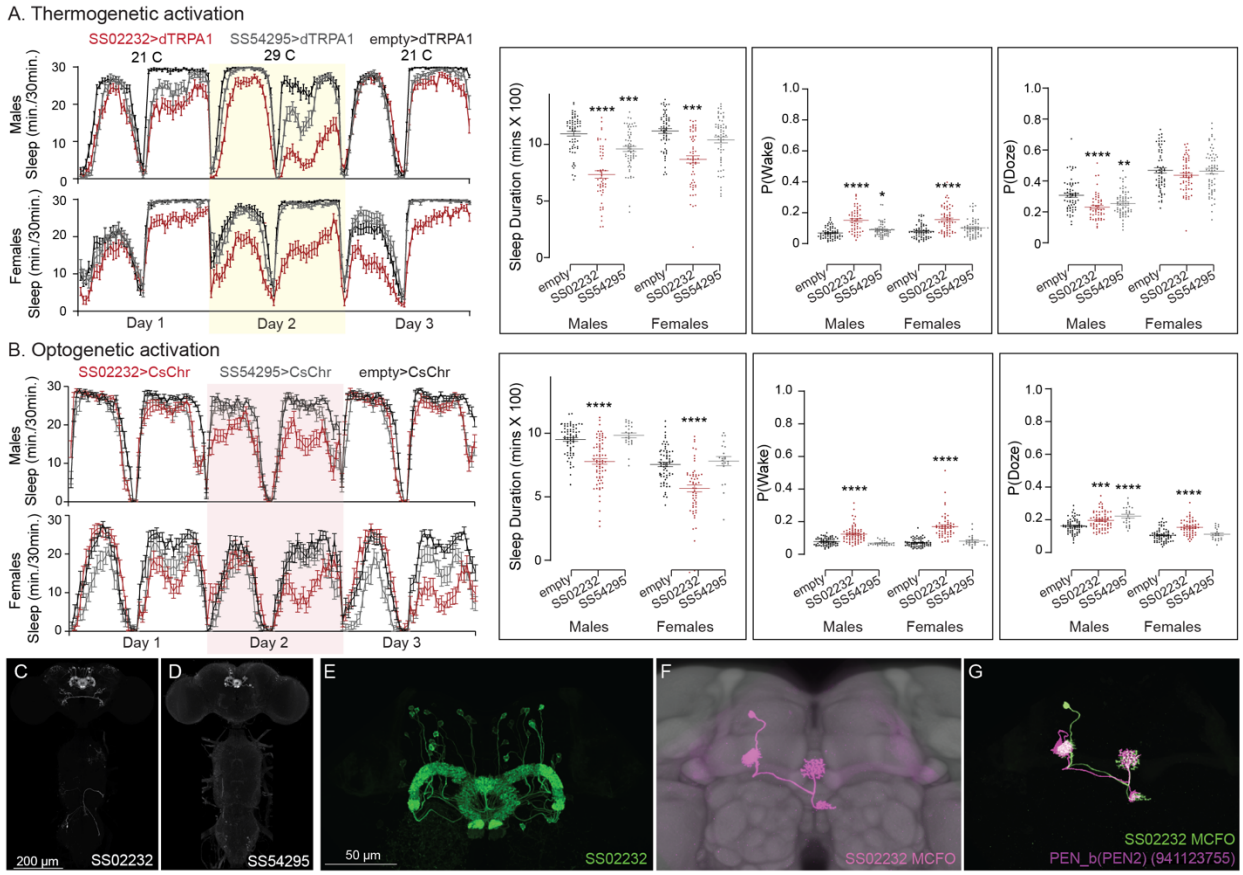

Figure 10—figure supplement 1. Activation phenotype of PEN_b, comprised of 22 columnar neurons linking the EB, PB and noduli (Wolff and Rubin 2018; Turner-Evans et al., 2020; Green et al., 2017; Hulse et al., 2021). Effects on activity of thermogenetic (A) and optogenetic (B) activation of PEN_b using split-GAL4 lines SS02232 and SS54295 is shown. Specifically, thermogenetic activation of these split-GAL4 lines decreases sleep duration and increases P(Wake) in males but only SS02232 is wake promoting in females. Optogenetic activation of SS02232 suppresses sleep and increases P(Wake) in both males and females supporting the general function of these neurons as wake-promoting. While both lines show high cell type specificity and minimal VNC expression, SS54295 has stochastic expression that might explain the weaker wake promoting effect seen with this line. (C-D) MIP images of GFP-driven expression in the brain and VNC of the two spilt-GAL4 lines. The brain and VNC are outlined in red. (E) Higher resolution images of the relevant brain area of SS02232. (F) Morphology of a single neuron revealed by stochastic labelling shown with neuropil reference. (G) Comparison of LM and EM cell morphologies. Original confocal stacks for panels C-F can be downloaded from www.janelia.org/split-gal4. The full genotypes of the driver lines are given there and in Supplementary File 1. Statistical comparisons were made by Kruskal-Wallis and Dunn's post hoc test. Asterisk indicates significance from 0: *p<0.05; **p<0.01; ***p<0.001; ****p<0.0001.

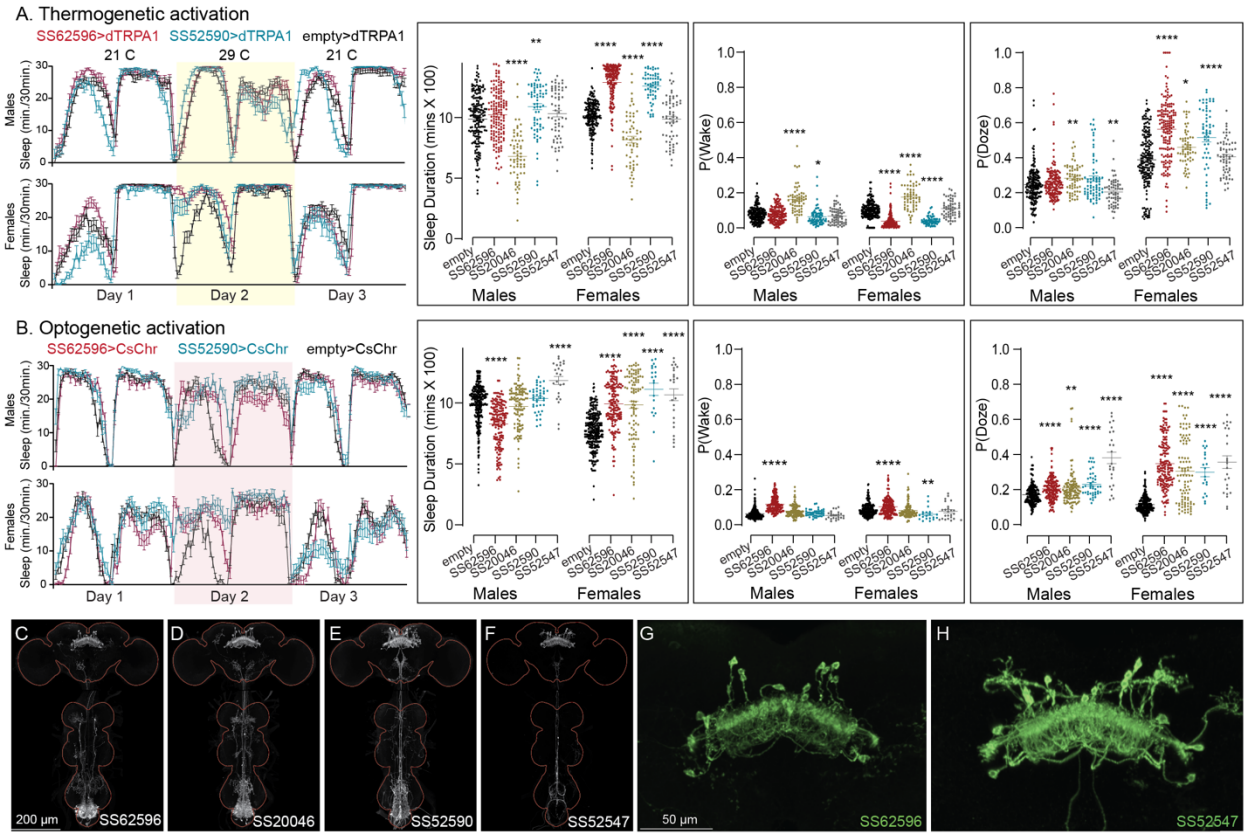

Figure 10—figure supplement 2. Activation phenotype of PFGs. Thermogenetic (A) and optogenetic (B) activation of PFGs reveals sexually dimorphic sleep behavior. We tested four different split-GAL4 lines for this cell type. All four lines display expression in the VNC complicating interpretation of the results. To mitigate this issue, we used lines with different hemidriver parents and visually distinct VNC expression patterns (C-F). The brain and VNC are outlined in red. Optogenetic activation (Day 2) in female flies showed increased sleep in all four driver lines and a mild increase in sleep duration in one of lines for male flies (SS52547). However, P(Doze) was consistently higher in male and female flies for all tested PFGs lines. Thermogenetic activation (Day 2) also shows sex specific phenotypes and two of the four lines (SS62596 and SS52590) have increased sleep. SS20046 has decreased sleep in females and male flies with dTRPA1 based activation but shows increased sleep with CsChrimson in females. Despite these inconsistencies, the data suggest a sex specific sleep promoting effect for this cell type. (G-H) Higher resolution images of the relevant brain area of SS62596 and SS52547. Original confocal stacks for panels C-H can be downloaded from www.janelia.org/split-gal4. The full genotypes of the driver lines are given there and in Supplementary File 1. Statistical comparisons were made by Kruskal-Wallis and Dunn's post hoc test. Asterisk indicates significance from 0: *p<0.05; **p<0.01; ***p<0.001; ****p<0.0001.

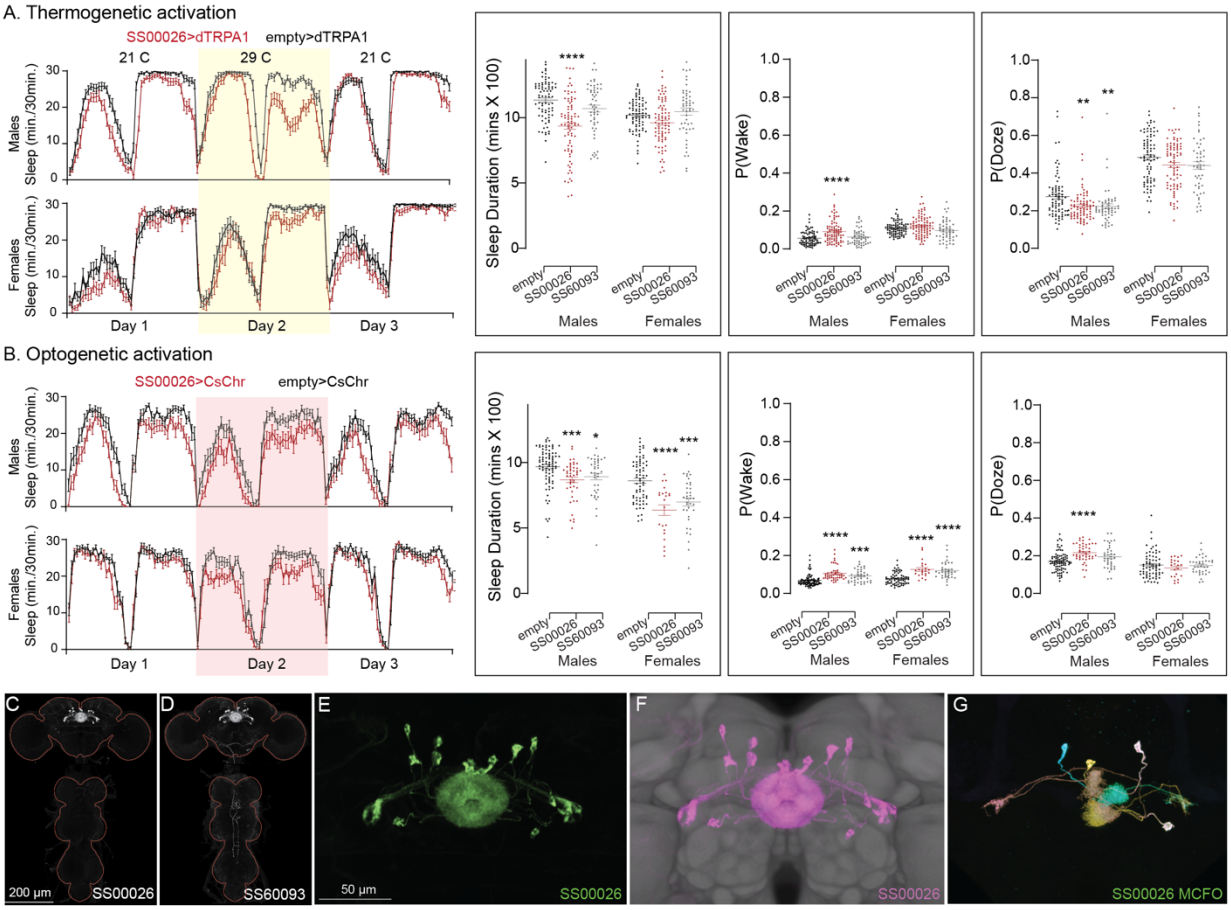

Figure 10—figure supplement 3. Thermogenetic activation (A) of EL neurons decreases sleep in one of the split-GAL4 lines (SS00026), while optogenetic activation (B) of both lines decreases sleep and increases P(Wake) on Day 2. (C,D) MIP images of GFP-driven expression in the brain and VNC of the three spilt-GAL4 lines. The brain and VNC are outlined in red. (E) Higher resolution images of the relevant brain area of in SS00026. (F) Same as panel E, but with neuropil reference. (G) Morphology of individual neurons revealed by stochastic labelling. Original confocal stacks for panels C-G can be downloaded from www.janelia.org/split-gal4. The full genotypes of the driver lines are given there and in Supplementary File 1. Statistical comparisons were made by Kruskal-Wallis and Dunn's post hoc test. Asterisk indicates significance from 0: *p<0.05; **p<0.01; ***p<0.001; ****p<0.0001.

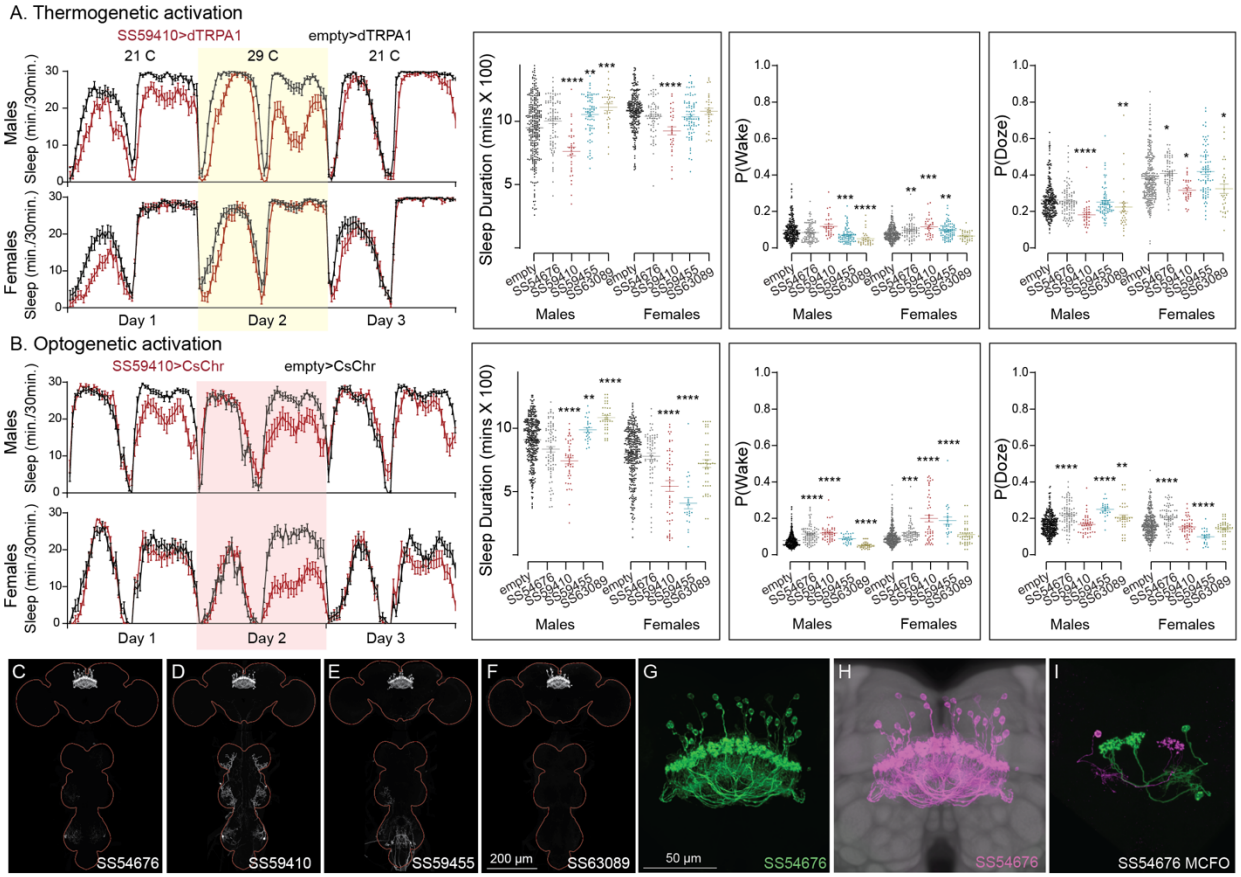

Figure 10—figure supplement 4. Activation phenotype of hDeltaK. This group of intrinsic columnar neurons is highly peptidergic and has been implicated in chronic social isolation-induced sleep loss (Li et al., 2021). We tested four split-GAL4 lines (SS59455, SS63089, SS54676 and SS59410). Our results do not give a consistent view of the role of this cell type in sleep regulation. (A) Thermogenetic activation of one of the four lines (SS59410) was wake-promoting in both sexes, while two (SS59455 and SS63089) were sleep-promoting in males, but not females. (B) Consistent with what was observed with thermogenetic activation, optogenetic activation of SS59410 also suppressed sleep in males and females, while SS59410 and SS59455 were sleep promoting in males, but not in females. (C-F) MIP images of GFP-driven expression in the brain and VNC of the four spilt-GAL4 lines. The brain and VNC are outlined in red. (G) Higher resolution images of the relevant brain area of in SS54676 (H) Same as panel G, but with neuropil reference. (I) Morphology of individual neurons revealed by stochastic labelling. We do not have any insight into the differences in behaviors between lines and cannot make an overall conclusion of their role in sleep regulation. Such line-to-line inconsistencies argue for caution in the interpretation of results, especially when only one line for a cell type has been assayed. Original confocal stacks for panels C-I can be downloaded from www.janelia.org/split-gal4. The full genotypes of the driver lines are given there and in Supplementary File 1. Statistical comparisons were made by Kruskal-Wallis and Dunn's post hoc test. Asterisk indicates significance from 0: *p<0.05; **p<0.01; ***p<0.001; ****p<0.0001.

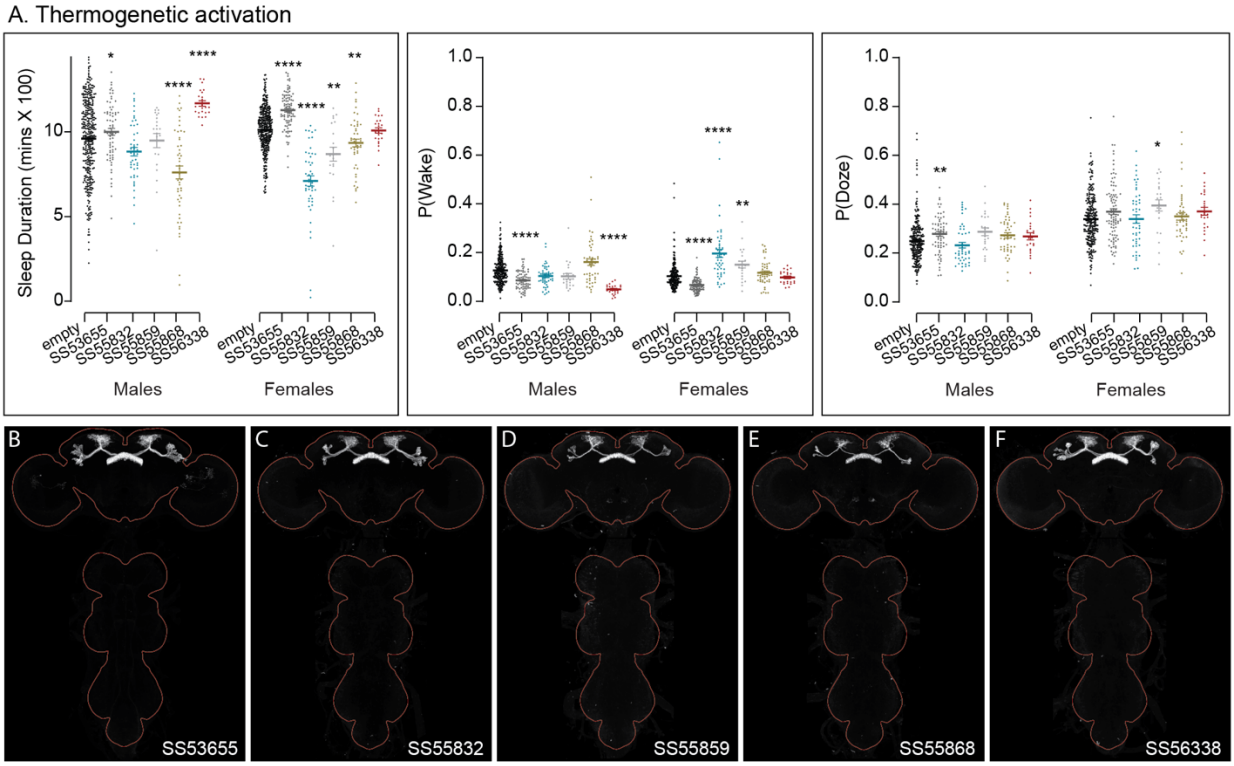

Figure 10—figure supplement 5. Activation phenotypes of combinations of dFB cell types. The five split-GAL4 lines used here each utilize R84C10 as one of their hemidrivers. They represent different (but largely overlapping subsets of layer 6 and 7 FB tangential cell types and have no detectable VNC expression. Jones et al. (2024) reported analysis of additional lines that used R84C10 as a hemidriver in split-GAL4 lines. We did not examine expression in other parts of the peripheral nervous system or muscle. (A) Thermogenetic activation revealed that some lines were sleep promoting and others wake promoting. (B-F) MIP images of GFP-driven expression in the brain and VNC of the four spilt-GAL4 lines. The brain and VNC are outlined in red. Original confocal stacks can be downloaded from www.janelia.org/split-gal4. The full genotypes of the driver lines are given there and in Supplementary File 1. Statistical comparisons were made by Kruskal-Wallis and Dunn's post hoc test. Asterisk indicates significance from 0: *p<0.05; **p<0.01; ***p<0.001; ****p<0.0001.

Our screen identified several cell types not previously associated with sleep and/or activity regulation. For example, hDeltaF was found to be strongly wake promoting (Figure 10). We also identified PEN_b (Figure 1—figure supplement 1), PFGs (Figure 1—figure supplement 2), EL (Figure 1—figure supplement 3) and hDeltaK (Figure 1—figure supplement 4) as likely to play a role. In most of these cases, we were able to assay multiple independent driver lines for the cell type. We also assayed several lines that each contained a mixture of dorsal FB cell types (Figure 1—figure supplement 5) but were otherwise free of contaminating brain or VNC expression. In addition to intrinsic components of the CX, we evaluated several cell types that, based on the connectome, we thought likely to convey information from the circadian clock to the CX. Figure 11 (SMP368) and Figure 11—figure supplement1 (SMP531) present two such cases of strongly wake promoting cell types.

Results for lines not discussed in detail in the main paper are provided as Supplementary Files. Supplementary Files 3 and 4 give results for 600 split-GAL4 lines assayed by thermogenetic activation with TRPA1 in both males and females, respectively. Supplementary Files 5 (males) and 6 (females) present results on over 200 lines, selected based on the results of thermogenetic activation, that were also assayed by optogenetic activation with CsChrimson. Images of the

expression patterns of these lines and their genotypes can be found at https://flylight-raw.janelia.org/. The set of lines is anatomically biased with the dorsal FB overrepresented, and many lines contain multiple cell types and non-CX expression. Nevertheless, we believe these data might be useful as a starting point for further exploration.

The goal of our screen was to identify candidate cell types that warranted further study. While we identified several new potential sleep regulating cell types within CX, we did not perform the additional characterization needed to elucidate the roles of these cell types. For example, we did not examine the effects of inhibiting their function. Nor did we examine parameters such as arousal thresholds or recovery from sleep deprivation. Finally, by using only a 24-hour activation protocol we might have missed features only observable in shorter activation protocols. On the other hand, we assayed all lines in both males and females with identical genetic and environmental manipulations and many lines were evaluated by both optogenetic and thermogenetic activation. We observed that many lines showed phenotypes that differed between sexes, even though the expression patterns of the split-GAL4 lines did not obviously differ across sexes. Lines that showed strong effects generally did so with both activation modes and with both beam crossing-based activity measures and video-based locomotion tracking.

Connections between the CX and the circadian clock.

Not surprisingly, the connectome reveals that many of the intrinsic CX cell types with sleep phenotypes are connected by wired pathways. The strongest of these connections are diagrammed in Figure 12, with Figure 12—figure supplement 1 also showing additional weaker connections. The connectome also suggested pathways from the circadian clock to the CX. Some of these have been previously noted. Links between clock output DN1 neurons to the ExR1 have been described in Lamaze et al. (2018) and Guo et al. (2018), and Liang et al. (2019) described a connection from the clock to ExR2 (PPM3) dopaminergic neurons. We found two SMP cell types, SMP368 and SMP531, that were very strongly wake-promoting when activated suggesting they might be components of previously undescribed wired pathways from the clock to the CX.

In addition to these wired pathways, our work supports the possibility of signaling from the clock over considerable distances to the CX using neuropeptides. Our RNA profiling of ER5 cells (Figure 9—figure supplement 1), which are known to be regulators of sleep and sleep homeostasis (Liu et al., 2016), revealed expression of receptors for both PDF and Dh44. The presence of the PDF receptor in ER5 cells was suggested by prior work (Im & Taghert, 2010; Parisky et al., 2008; Pirez et al., 2013). We confirmed these observations and showed that ER5 cells make Dh31 (video 1). Dh44 has been implicated as a clock output that regulates locomotor activity rhythms (Barber et al., 2021; Cavanaugh et al., 2014) and the DH44R1 receptor has been shown to function in sleep regulation in non-CX cells (King et al., 2017). However, the presence of the Dh44R2 receptor in the EB was unexpected. Dh31 is expressed by many cells in the fly brain (see Figure 6F) including DN1s (Kunst et al., 2014) and has been shown to play a role in sleep regulation; the cellular targets of Dh31 released from ER5 are unknown, however previous work (Goda et al., 2017; Mertens et al., 2005; Shafer et al., 2008) has shown that Dh31 can activate the PDF receptor raising the possibility of autocrine signaling. Andreani et al. (2022) also showed a functional link between the clock and ER5 cells, but the circuit mechanism was not elucidated.

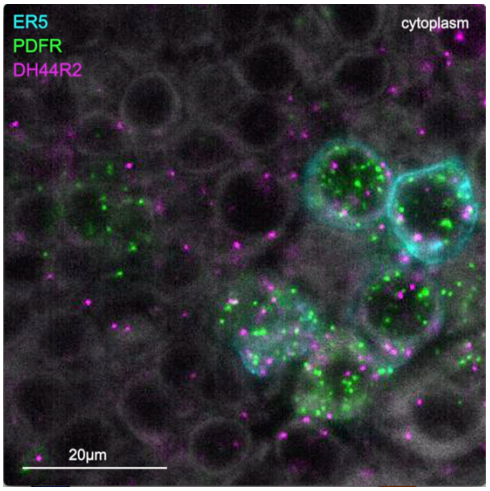

Video 1. Expression of genes encoding the neuropeptide receptors PDFR and Dh44R2 as well as the neuropeptide Dh31 in ER5 cells of the EB. The ER5 cells were marked by membrane bound GFP expression and expression of PDFR, Dh44R2 and Dh31 were assayed by EASI-FISH.

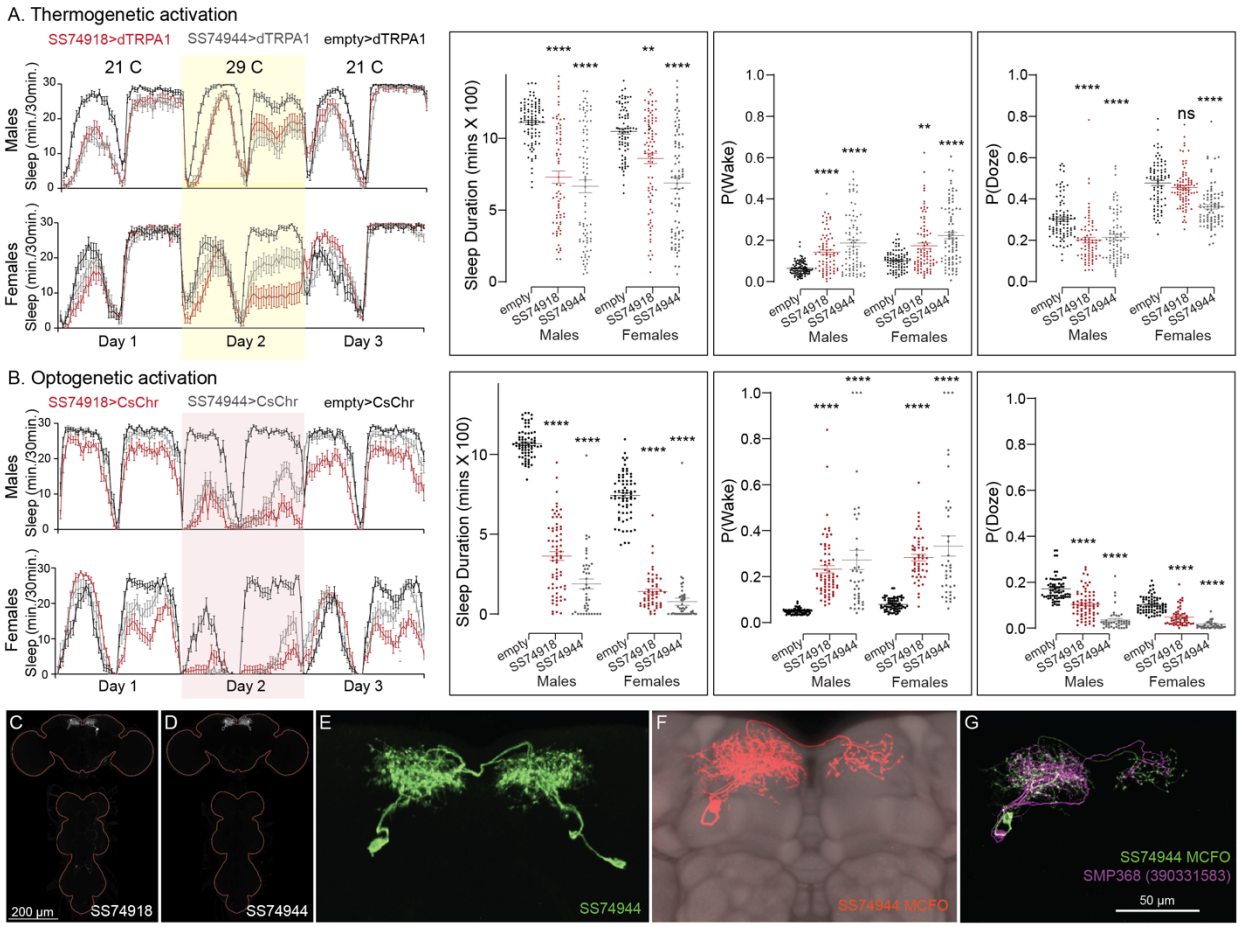

Figure 11. Activation of SMP368 decreases sleep. SMP368 connects central clock outputs to the CX (see Figure 12 and Figure 12—figure supplement 1). Both split-GAL4 lines for SMP368 that we tested (SS74918 and SS74944) are strongly wake-promoting in both thermogenetic (A) and optogenetic (B) activation and the phenotypes are consistent across sexes. Further, these lines show increase P(Wake) and decreased P(Doze) indicative of decreased sleep pressure and altered sleep depth. (C-D) MIP images of GFP-driven expression in the brain and VNC of the two spilt-GAL4 lines. The brain and VNC are outlined in red. (E) Higher resolution images of the relevant brain area of SS74944. (F) Morphology of a single neuron revealed by stochastic labelling shown with neuropil reference. (G) Comparison of LM and EM cell morphologies. Original confocal stacks for

panels C-F can be downloaded from www.janelia.org/split-gal4. The full genotypes of the driver lines are given there and in Supplementary File 1. Statistical comparisons were made by Kruskal-Wallis and Dunn's post hoc test. Asterisk indicates significance from 0: **p<0.01; ****p<0.0001.

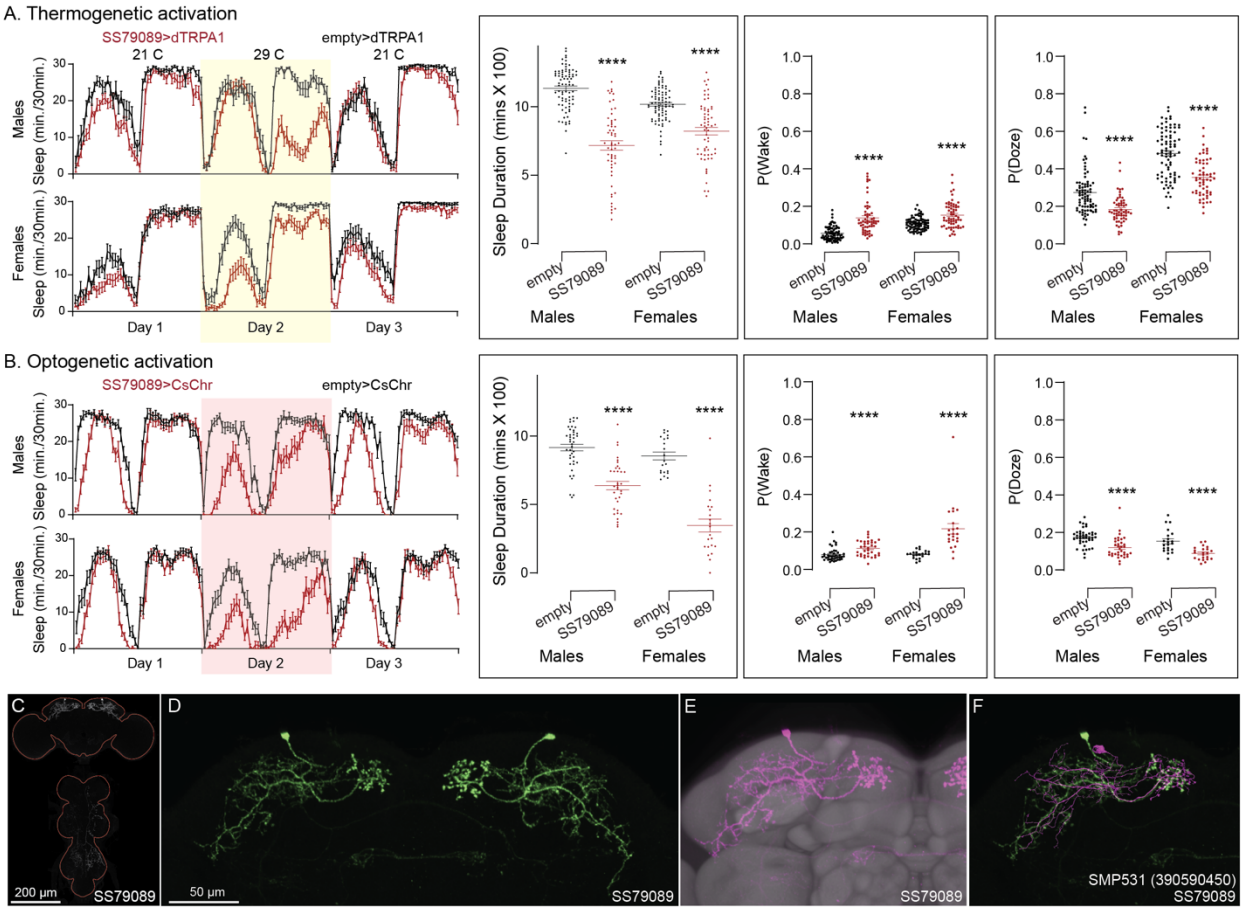

Figure 11—figure supplement 1. Activation phenotype of SMP531. SMP531 is part of a potential pathway from clock outputs to the CX (see Figure 12—figure supplement 1) The SMP531 split-GAL4 line SS79089 suppresses sleep when activated thermogenetically (A) and optogenetically (B) in both males and females. Further, activation of this line increases P(Wake) and decreased P(Doze). (C) MIP image of GFP-driven expression in the brain and VNC of SS79089. The brain and VNC are outlined in red. (D) Higher resolution images of the relevant brain area of SS79089. (E) Morphology shown with neuropil reference. (F) Comparison of LM and EM cell morphologies. Original confocal stacks for panels C-E can be downloaded from www.janelia.org/split-gal4. The full genotypes of the driver lines are given there and in Supplementary File 1. Statistical comparisons were made by Kruskal-Wallis and Dunn's post hoc test. Asterisk indicates significance from 0: ****p<0.0001.

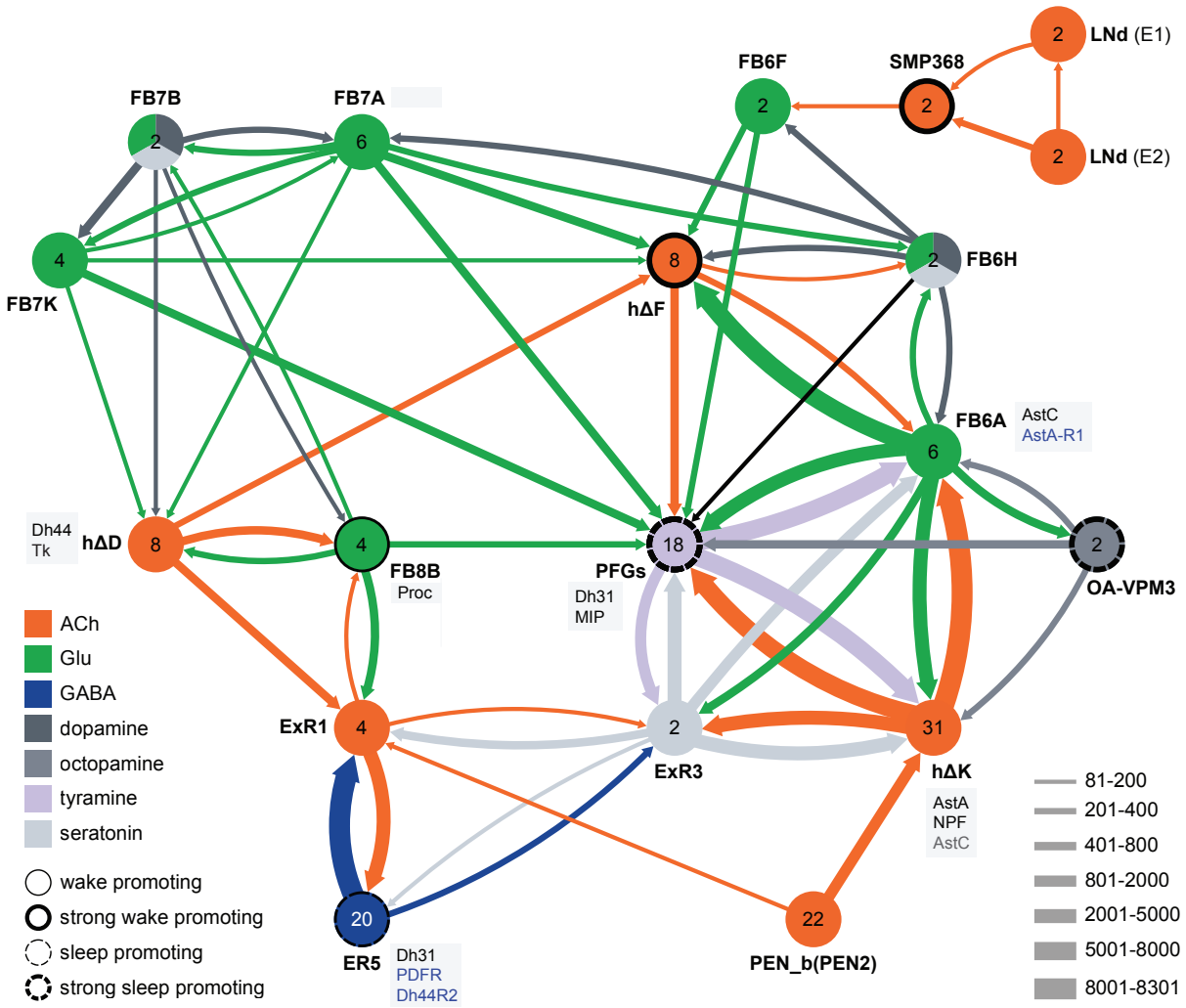

Figure 12. Circuit diagram of CX cells implicated in regulating sleep. Selected CX cell types, plus non-CX cell types SMP368, LNd and OA-VPM3, are shown. The number within each circle denotes the number of cells in that cell type. The neurotransmitters used by each cell type are indicated by color coding, and the number of synapses between cell types is represented by arrow width. Cell types that have been shown to promote sleep or wake when activated are indicated. Experimental evidence for the wake promoting effects of OA-VPM3 is from Reyes, M and Sitaraman D (in preparation). In cases where we have experimentally determined expression of neuropeptides or neuropeptide receptor genes by either EASI-FISH or RNA profiling, this information is indicated in the boxes next to the relevant cell type. Cell type names are from the hemibrain release 1.2.1 except for the LNd neurons whose names have been modified based on morphology and connectivity; they have been grouped into two types: LNd (E1) corresponds to hemibrain body IDs 5813056917 + 5813021192 and LNd (E2) corresponds to hemibrain body IDs 511051477 (5th LNv) + 5813069648 (LNd6) (Shafer et al., 2022). Because the CX is a central body and the inputs from CX cells that have their soma in right or left hemisphere appear to be comingled on their downstream targets, the synaptic strengths shown represent the combined number of cells of each type, regardless of soma position. For example, the arrow thickness between FB6F and hDeltaF reflects the total number of synapses (368) from FB6F_R and FB6F_L to all hDeltaF cells; the individual synapse number between each of the two FB6F cells to each of the eight hDeltaF cells, which ranges from 7 to 39, can be found in neuPrint. The sole exception is the LNd cells where the synaptic strength represents only the output of LNds in the right hemisphere. See Figure 53 of Hulse et al. (2021) for additional connected cells.

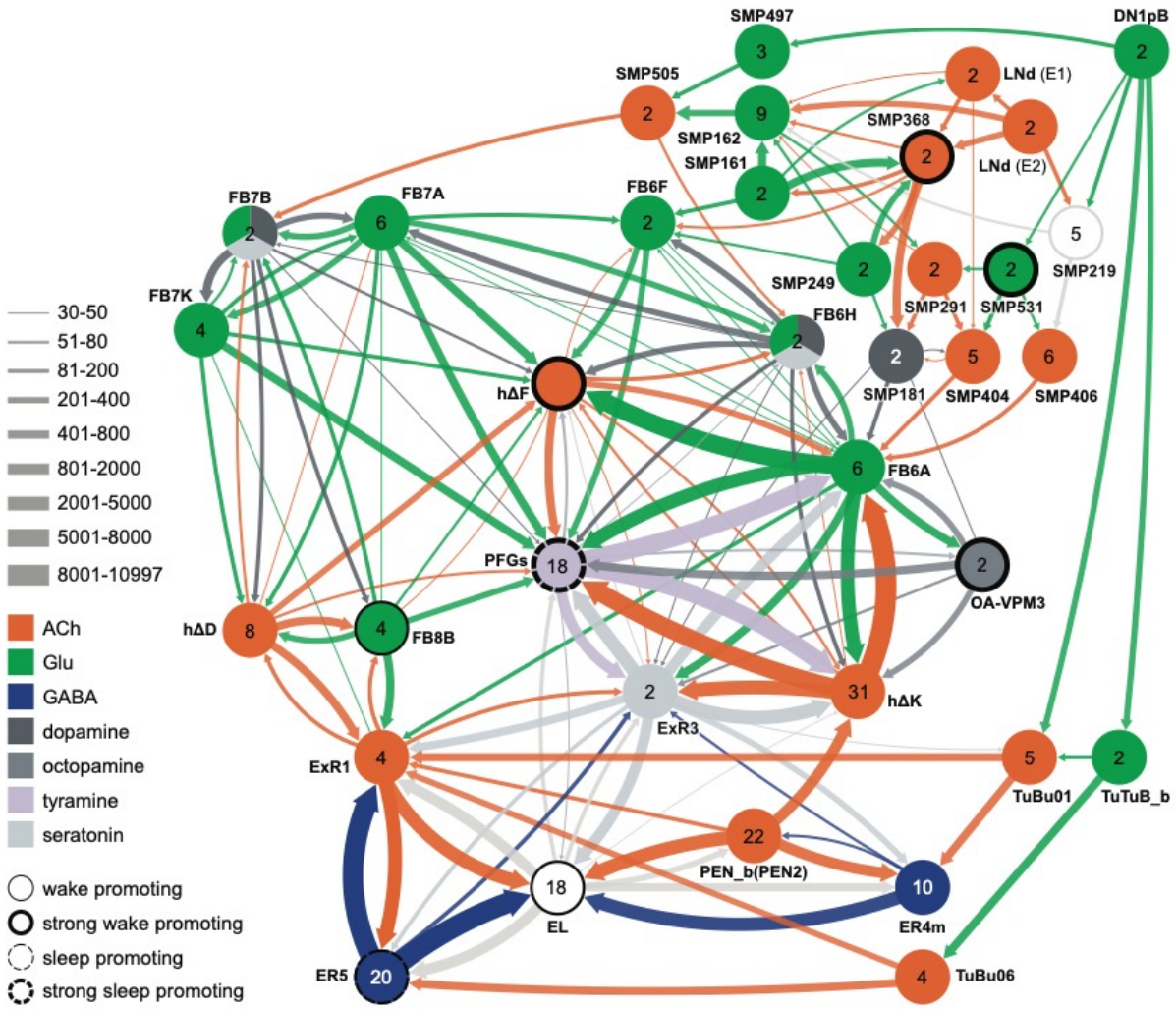

Figure 12—figure supplement 1. Circuit diagram showing some additional cell types potentially involved in regulating sleep. Other studies have identified roles for some of these cell types as well as additional cells not shown in this diagram. Links between clock output DN1 neurons to the ExR1 have been described in Lamaze et al. (2018) and Guo et al. (2018). Liang et al. (2019) described a connection form the clock to ExR2 (PPM3) dopaminergic neurons.

Concluding Remarks

We provide a greatly enhanced set of genetic reagents for manipulating the intrinsic cell types of the CX that will be instrumental in fully elucidating the many functions of the CX. We illustrate their use in discovering cell types involved in activity regulation, and uncovered new potential wired and peptidergic connections between the circadian clock and the CX. We surveyed neuropeptide and neuropeptide receptor gene expression in the adult central brain. Neuropeptides fell into two broad categories, those at are expressed in only a few cells and those that are expressed in dozens to hundreds of cells. We observed that neuropeptide receptor genes were much more broadly expressed than those of their cognate neuropeptides. Finally, we generated the largest available dataset of co-expression of neuropeptides and neurotransmitters in identified cell types. Unexpectedly, we found that all neuropeptide-expressing cell types also expressed a small neurotransmitter. Our data reveal the pervasive potential for peptidergic communication within the CX—more than half of the cell types we examined expressed a neuropeptide and one-third of those expressed multiple neuropeptides.

Materials and Methods

Generation of split-GAL4 lines. Split-GAL4 lines were generated as previously described (Dionne et al. 2018). Databases of expression patterns generated in the adult brain by single genomic fragments cloned upstream of GAL4 (Jennet et al., 2012; Tirian et al., 2012) were manually or computationally (Meissner et al., 2023) screened. Individual enhancers that showed expression in the desired cell type were then cloned into vectors that contained either the DNA-binding or activation domain of GAL4 (Luan et al, 2008; Pfeiffer et al., 2012). These constructs were combined in the same individual and screened for expression in the desired cell type by confocal imaging. Over 15,000 such screening crosses were performed to generate the new split-GAL4 lines reported here. Successful constructs were made into stable lines.

The lines listed in Supplementary File 1 are currently being maintained at Janelia and the majority of these have also been deposited in the Bloomington Drosophila Stock Center.

Characterization of split-GAL4 lines. Lines were characterized by confocal imaging of the entire expression pattern in the brain and VNC at 20X. Most lines were also imaged at higher magnification (63x) and/or subjected to stochastic labelling (MCFO; Nern et al., 2015) to reveal the morphology of individual cells. Split-GAL4 images are shown as MIPs after alignment to JRC2018 (Bogovic et al., 2020). Over 1,800 confocal stacks derived from over 450 lines generated during this work are presented in, and can be downloaded from, an on-line database (janelia.org/split-GAL4). Images for the additional lines used in the sleep screen are available from flylight-raw.janelia.org.

Determining the correspondence between the cell-types present in each split-GAL4 line and those described in the connectome (Hulse et al., 2021) was based solely on morphology. Even when assigning correspondence between cells in two different connectomes, where information on connectivity can also be employed, the process is not always straightforward (see Schlegel et al. 2024). Because of the similarity in morphology of many of the CX cell types it was often challenging to assign correspondence to the cell types defined by connectome analysis. For this reason, we rated our confidence in our assignments as Confident, Probable or Candidate and include this information for each line at janelia.org/split-GAL4. To be considered confident, we judged our opinion had a >95% chance of being correct. Such assignments were generally only possible for cell types which had morphological features clearly distinct from those in other cell types. Most assignments were rated as Probable indicating 70-95% confidence. Lines whose cell type assignments are listed as Probable have been rigorously examined and the assignments are the most accurate that the available data allow. In the absence of single-cell data available in MCFO brains (the case for many lines) or additional data (for example, physiological data on connectivity), cell types that are morphologically very similar cannot be distinguished with complete confidence. Lines whose cell type assignments are listed as Candidate are even less certain (30-70% confidence).

RNA *in situ* hybridization. Adult females (5 to 7 days post eclosion) were expanded, probed, and imaged using the EASI-FISH method as described in (Eddison and Ihrke, 2022; Close et al., under review). The oligo probes and HCR hairpins were designed by, and purchased from, Molecular Instruments, Inc. Imaging was performed on a Zeiss Z7 microscope equipped with a 20X objective. Laser power and exposure time was optimized to maximize the signal-to-noise ratio. For neurotransmitters, the specific probes used for each cell type are indicated in Figure 9 and in Supplemental File 1. For neuropeptides, each of the 17 selected NP probes shown in Figure 5—figure supplement 1 was used on all cell types in Figure 9 except those marked by "—" in the neuropeptide column.

RNA profiling. The data shown in Figure 9—Figure supplement 1 were generated as described in Aso et al. 2019. See NCBI Gene Expression Omnibus (accession number GSE271123) for the raw data and additional details.

Sleep measurement and analysis: Thermogenetic activation screen. Split-GAL4 flies were crossed to 10X UAS-dTrpA1 (attP16) (Hamada et al. 2008) and maintained at 21–22°C in vials containing standard dextrose-based media (7.9g Agar, 27.5g Yeast, 52g cornmeal, 110g dextrose, 8.75 ml 20% Tegosept and 2 ml propionic acid/ liter).

Virgin female progeny or male progeny (as specified in the figures), 3–7 days post-eclosion, (n = 16-32/trial) were placed in 65 mm × 5 mm transparent plastic tubes with standard cornmeal dextrose agar media and placed in a Drosophila Activity Monitoring system (Trikinetics). Food composition was kept consistent between rearing and experimentation. Locomotor activity data were collected in 1-min bins for 5-7 days. Activity monitors were maintained with a 12 hr:12 hr light–dark cycle at 40-65% relative humidity. Total 24-hr sleep amounts (daytime plus nighttime sleep duration), Pwake, and Pdoze were extracted from the locomotor data as described in (Donelson et al., 2012; Wiggin et al., 2020) using MATLAB-based SCAMP program. (Sitaraman et al., 2024; Vecsey et al., 2024)

Sleep duration was defined as 5 min or more of inactivity (Hendricks et al., 2000; Shaw et al., 2000). Representative sleep profiles were generated representing average (n = 24–32) sleep (min/30 min) for day 1 (baseline), day 2 (activation), and day 3 (recovery/post activation). In addition to permissive temperature controls, split-pBDPGAL4U /dTrpA1 were used as genotypic controls for hit detection. pBDPGAL4U (attP40, attP2), has enhancerless GAL4-AD construct and GAL4-DBD constructs inserted on chromosome II and III (Dionne et al., 2018), as is the case for split-GAL4 driver lines in behavioral assays. Each split-GAL4 line was tested at least twice in independent trials. For all screen hits, wake activity was calculated as the number of beam crossings/min when the fly was awake. Statistical comparisons between experimental and control genotypes were performed using Prism (Graphpad Inc) by Kruskal Wallis One way ANOVA followed by Dunn's post-test. Pairwise comparisons between the empty (split-pBDPGAL4U) control and experimental lines were made using Mann-Whitney U test.

Sleep measurement and analysis: Optogenetic activation screen. Split-GAL4 flies were crossed to 20XUAS-CsChrimson-mVenus-trafficked (attP18) (BDSC:55134) and maintained at 21–25°C in vials containing standard cornmeal food supplemented with 0.2% retinal. Male and virgin female progeny were collected into separate vials containing standard cornmeal food with 0.4% added retinal and kept in a 25°C incubator on a 12:12 light:dark schedule for 3-5 days before loading. Typical sleep experiments lasted 6-7 days. Flies were loaded into 96 well plates or individual tubes using CO2 anesthesia. Flies were allowed to recover from anesthesia and acclimatize to the experimental chambers for 16-18 hours prior to starting the experiment.

The behavioral setup for video recording system was adapted from (Guo et al., 2016). Flies were briefly anesthetized and loaded into 96 well plates (Falcon™ 96-Well, Non-Treated, Fisher Scientific Inc) containing 150 ml per well of 5% sucrose, 1% agarose and 0.4% retinal. The plates were covered with breathable sealing films. Small holes (one per well) were poked with fine forceps into the film to further ensure air exchange and prevent condensation. The entire setup was housed in an incubator to control light/dark conditions and temperature. The 96-well plates with flies were placed in holders, constantly illuminated from below using an 850 nm LED board (Smart Vision Lights Inc) and imaged from above using a FLIR Flea 3 camera (Edmund Optics Inc). 635 nm red light (for optogentic activation) was provided using an additional backlight, low levels of white light (to provide a light-dark cycle) were supplied from above. Optogenetic activation was for a 24 h period (starting in the morning at the same time as the white light was turned on for the day) and was delivered in pulses of 25 ms duration at 2 Hz frequency. Each experiment also included at least one full day without the

red light preceding and following the activation day (matching the general design of the thermogenetic experiments).

Fly movement was tracked using single fly position tracker (GitHub - cgoina/pysolo-tools) and processed for sleep duration and other sleep parameters using SCAMP. In addition to the 5 min criteria, used to define total duration of sleep, P(Doze), the probability that an active fly will stop moving, and P(Wake), the probability that a stationary fly will start moving provide key additional measures of inactivity and activity and were included in our analyses (Wiggin et al., 2020). These sleep measures are presented in Figure 10 and 11 (and supplements) and supplementary files 3,4,5, and 6.

Supplemental Files for sleep phenotypes: The supplemental files present data on day1 (baseline) and day 2 (activation). Given the large effects of environmental conditions on activity, we calculated p values between experimental and control group within the same environmental conditions. However, we also present mean differences between the days as a complementary way to identify lines that modified sleep when activated.

Acknowledgements

We thank Y. Aso (SS32244), J. Goldammer (SS51128), and M. Ito (SS49931, SS48762) for providing GAL4 lines. Robert Ray performed the RNA profiling experiments summarized in Figure 9—figure supplements 1 and 2 and the meta-analysis of RNA profiling data to identify which neuropeptide genes were expressed in the adult brain. Marisa Dreher (Dreher Design Studios) performed connectomic analyses and figure generation. We thank Janelia's Project Technical Resources led by Gudrun Ihrke for assistance: ME, NC; Kari Close and Yisheng He performed EASI-FISH experiments, and Claire Managan scored results; Dan Bushey helped with earlier versions of python scripts to collate sleep assay data sets. Jennifer Jeter imaged and scored EASI-FISH experiments. Janelia's FlyLight Project Team and Project Pipeline Support team, especially Allison Vannan, Jennifer Jeter, Joanna Hausenfluck, Zachary Dorman, Kelley Lee, and Geoffrey Meissner, performed CNS dissections, staining, and imaging. Janelia's Invertebrate Shared Resource and Scientific Computing contributed to stock generation and image processing, respectively. Geoffrey Meissner and Rob Svirskas contributed to the split-GAL4 website. Michael Kunst, Preeti Sareen and Michael Nitabach contributed to early screening of split-GAL4 lines for effects on sleep. Wyatt Korff helped with establishment of the 96-well sleep assay. Heather Dionne, Martin Reyes, Anisha Ali and Matthew Finger helped with conducting sleep experiments and analyzing data. We thank Brad Hulse, Alexander Bates, Gabi Maimon, Maria de la Paz, Dick Nässel, Mubarak Hussain Syed and members of the Rosbash lab for comments on earlier drafts of the manuscript and for helpful discussion. This work was supported by the Howard Hughes Medical Institute, NIH 2R15GM125073-03 (to D.S.), and NSF IOS 2042873 (to D.S.).

Author Contributions

TW, ME, DS and GMR conceived the study. TW, AN and GMR created split-GAL4 lines. TW analyzed lines for CX cell types, assigned them to cell types, and scored EASI-FISH experiments. ME designed, conducted, and scored EASI-FISH experiments. NC, PS and DS designed and conducted behavioral assays. GMR wrote the paper with input from all authors.

References

Andreani T, Rosensweig C, Sisobhan S, Ogunlana E, Kath W, Allada R. Circadian programming of the ellipsoid body sleep homeostat in *Drosophila*. Elife. 2022 Jun 23;11:e74327. doi: 10.7554/eLife.74327. PMID: 35735904.

Aso Y, Hattori D, Yu Y, Johnston RM, Iyer NA, Ngo TT, Dionne H, Abbott LF, Axel R, Tanimoto H, Rubin GM. The neuronal architecture of the mushroom body provides a logic for associative learning. Elife. 2014 Dec 23;3:e04577. doi: 10.7554/eLife.04577. PMID: 25535793.

Aso Y, Ray RP, Long X, Bushey D, Cichewicz K, Ngo TT, Sharp B, Christoforou C, Hu A, Lemire AL, Tillberg P, Hirsh J, Litwin-Kumar A, Rubin GM. Nitric oxide acts as a cotransmitter in a subset of dopaminergic neurons to diversify memory dynamics. Elife. 2019 Nov 14;8:e49257. doi: 10.7554/eLife.49257.

Barber AF, Fong SY, Kolesnik A, Fetchko M, Sehgal A. *Drosophila* clock cells use multiple mechanisms to transmit time-of-day signals in the brain. ProcNatl Acad Sci U S A. 2021 Mar 9;118(10):e2019826118. doi:10.1073/pnas.2019826118. PMID: 33658368.

Bargmann CI, Marder E. From the connectome to brain function. Nat Methods. 2013 Jun;10(6):483-90. doi: 10.1038/nmeth.2451. PMID: 23866325.

Bogovic JA, Otsuna H, Heinrich L, Ito M, Jeter J, Meissner G, Nern A, Colonell J, Malkesman O, Ito K, Saalfeld S. An unbiased template of the Drosophila brain and ventral nerve cord. PLoS One. 2020 Dec 31;15(12):e0236495. doi: 10.1371/journal.pone.0236495. PMID: 33382698

Cavanaugh DJ, Geratowski JD, Wooltorton JR, Spaethling JM, Hector CE, Zheng X, Johnson EC, Eberwine JH, Sehgal A. Identification of a circadian output circuit for rest:activity rhythms in Drosophila. Cell. 2014 Apr 24;157(3):689-701. doi: 10.1016/j.cell.2014.02.024. PMID: 24766812.

Chen N, Zhang Y, Rivera-Rodriguez EJ, Yu AD, Hobin M, Rosbash M, Griffith LC. Widespread posttranscriptional regulation of cotransmission. Sci Adv. 2023 Jun 2;9(22):eadg9836. doi: 10.1126/sciadv.adg9836. Epub 2023 Jun 2. PMID: 37267358.

Close K, He Y, Jeter J, Ihrke G, Eddison M. Multiplex Detection of Gene Expression in the Intact Drosophila Brain using EASI-FISH 2024 submitted to Jove.

Davies K, Janssens J, Koldere D, De Waegeneer M, Pech U, Kreft Ł, Aibar S, Makhzami S, Christiaens V, Bravo González-Blas C, Poovathingal S, Hulselmans G, Spanier KI, Moerman T, Vanspauwen B, Geurs S, Voet T, Lammertyn J, Thienpont B, Liu S, Konstantinides N, Fiers M, Verstreken P, Aerts S. A Single-Cell Transcriptome Atlas of the Aging Drosophila Brain. Cell. 2018 Aug 9;174(4):982-998.e20. doi: 10.1016/j.cell.2018.05.057. Epub 2018 Jun 18. PMID: 29909982.

Dionne H, Hibbard KL, Cavallaro A, Kao JC, Rubin GM. Genetic Reagents for Making Split-GAL4 Lines in Drosophila. Genetics. 2018 May;209(1):31-35. doi: 10.1534/genetics.118.300682. Epub 2018 Mar 13. PMID: 29535151.

Donelson N, Kim EZ, Slawson JB, Vecsey CG, Huber R, Griffith LC. 2012. High-resolution positional tracking for long-term analysis of Drosophila sleep and locomotion using the “tracker” program. *PLoS One* 7. doi:10.1371/journal.pone.0037250

Dubowy C, Sehgal A. Circadian Rhythms and Sleep in *Drosophila melanogaster*. Genetics. 2017 Apr;205(4):1373-1397. doi:10.1534/genetics.115.185157. PMID: 28360128.

Eckstein N, Bates AS, Champion A, Du M, Yin Y, Schlegel P, Lu AK, Rymer T, Finley-May S, Paterson T, Parekh R, Dorkenwald S, Matsliah A, Yu SC, McKellar C, Sterling A, Eichler K, Costa M, Seung S, Murthy M, Hartenstein V, Jefferis GSXE, Funke J. Neurotransmitter classification from electron microscopy images at synaptic sites in Drosophila melanogaster. Cell. 2024 May 9;187(10):2574-2594.e23. doi: 10.1016/j.cell.2024.03.016. PMID: 38729112.

Eddison M and Ihrke G. Expansion-assisted iterative fluorescence in situ hybridization (EASI-FISH) in Drosophila CNS. Protocols.io.2022. doi: dx.doi.org/10.17504/protocols.io.5jyl8jmw7g2w/v1

Epiney D, Chaya GNM, Dillon NR, Lai S-L, Doe CQ Transcriptional complexity in the insect central complex: single nuclei RNA sequencing of adult brain neurons derived from type 2 neuroblasts 2013 www.biorxiv.org/content/10.1101/2023.12.10.571022v1.full.pdf

Fisher YE. Flexible navigational computations in the Drosophila central complex. Curr Opin Neurobiol. 2022 Apr;73:102514. doi:10.1016/j.conb.2021.12.001. Epub 2022 Feb 20. PMID: 35196623.

Goda T, Tang X, Umezaki Y, Chu ML, Kunst M, Nitabach MNN, Hamada FN. Drosophila DH31 Neuropeptide and PDF Receptor Regulate Night-Onset Temperature Preference. J Neurosci. 2016 Nov 16;36(46):11739-11754. doi: 10.1523/JNEUROSCI.0964-16.2016. PMID: 27852781.

Green J, Adachi A, Shah KK, Hirokawa JD, Magani PS, Maimon G. A neural circuit architecture for angular integration in Drosophila. Nature. 2017 Jun1;546(7656):101-106. doi: 10.1038/nature22343. Epub 2017 May 22. PMID: 28538731.

Green J, Maimon G. Building a heading signal from anatomically defined neuron types in the Drosophila central complex. Curr Opin Neurobiol. 2018 Oct;52:156-164. doi: 10.1016/j.conb.2018.06.010. Epub 2018 Jul 18. PMID:30029143.

Guo F, Holla M, Díaz MM, Rosbash M. A Circadian Output Circuit Controls Sleep-Wake Arousal in Drosophila. Neuron. 2018 Nov 7;100(3):624-635.e4. doi:10.1016/j.neuron.2018.09.002. Epub 2018 Sep 27. PMID: 30269992.

Hamada FN, Rosenzweig M, Kang K, Pulver SR, Ghezzi A, Jegla TJ, Garrity PA. An internal thermal sensor controlling temperature preference in Drosophila. Nature. 2008 Jul 10;454(7201):217-20. doi: 10.1038/nature07001. Epub 2008 Jun 11. PMID: 18548007.

Hamid A, Gattuso H, Caglar AN, Pillai M, Steele T, Gonzalez A, Nagel K, Syed MH. The conserved RNA-binding protein Imp is required for the specification and function of olfactory navigation circuitry in Drosophila. Curr Biol. 2024 Feb 5;34(3):473-488.e6. doi: 10.1016/j.cub.2023.12.020. Epub 2024 Jan 4. PMID: 38181792.

Hendricks JC, Finn SM, Panckeri KA, Chavkin J, Williams JA, Sehgal A, Pack AI. 2000. Rest in Drosophila is a sleep-like state. *Neuron* 25. doi:10.1016/S0896-6273(00)80877-6

Hulse BK, Haberkern H, Franconville R, Turner-Evans DB, Takemura SY, Wolff T, Noorman M, Dreher M, Dan C, Parekh R, Hermundstad AM, Rubin GM, Jayaraman V. 2021. A connectome of the drosophila central complex reveals network motifs suitable for flexible navigation and context-dependent action selection. *Elife* 10. doi:10.7554/eLife.66039

Im SH, Taghert PH. PDF receptor expression reveals direct interactions between circadian oscillators in Drosophila. J Comp Neurol. 2010 Jun 1;518(11):1925-45. doi: 10.1002/cne.22311. PMID: 20394051.

Jones JD, Holder BL, Montgomery AC, McAdams CV, He E, Burns AE, Eiken KR, Vogt A, Velarde AI, Elder AJ, McEllin, JA Dissel S. The dorsal fan-shaped body is a neurochemically heterogeneous sleep-regulating center in *Drosophila*. bioRxiv 2024.04. 10.588925.

Jenett A, Rubin GM, Ngo TT, Shepherd D, Murphy C, Dionne H, Pfeiffer BD,Cavallaro A, Hall D, Jeter J, Iyer N, Fetter D, Hausenfluck JH, Peng H, Trautman ET, Svirskas RR, Myers EW, Iwinski ZR, Aso Y, DePasquale GM, Enos A, Hulamm P, Lam SC, Li HH, Laverty TR, Long F, Qu L, Murphy SD, Rokicki K, Safford T, Shaw K, Simpson JH, Sowell A, Tae S, Yu Y, Zugates CT. A GAL4-driver line resource for Drosophila neurobiology. Cell Rep. 2012 Oct 25;2(4):991-1001. doi: 10.1016/j.celrep.2012.09.011. Epub 2012 Oct 11. PMID: 23063364.

Kahsai L, Winther, Å M. 2011. Chemical neuroanatomy of the *Drosophila* central complex: distribution of multiple neuropeptides in relation to neurotransmitters. *J Comp Neurol* 519**,** 290-315.

Keram P. The neuronal building blocks of the navigational toolkit in the central complex of insects. Current Opinion in Insect Science. 2022.

King AN, Barber AF, Smith AE, Dreyer AP, Sitaraman D, Nitabach MN, Cavanaugh DJ, Sehgal A. A Peptidergic Circuit Links the Circadian Clock to Locomotor Activity. Curr Biol. 2017 Jul 10;27(13):1915-1927.e5. doi:10.1016/j.cub.2017.05.089. Epub 2017 Jun 29. PMID: 28669757.

Kunst M, Hughes ME, Raccuglia D, Felix M, Li M, Barnett G, Duah J, Nitabach MN. Calcitonin gene-related peptide neurons mediate sleep-specific circadian output in Drosophila. Curr Biol. 2014 Nov 17;24(22):2652-64. doi:10.1016/j.cub.2014.09.077. Epub 2014 Oct 30. PMID: 25455031.

Lamaze A, Krätschmer P, Chen KF, Lowe S, Jepson JEC. 2018. A Wake-Promoting Circadian Output Circuit in Drosophila. *Current Biology* 28. doi:10.1016/j.cub.2018.07.024

Lee G, Jang H, Oh Y. The role of diuretic hormones (DHs) and their receptors in Drosophila. BMB Rep. 2023 Apr;56(4):209-215. doi: 10.5483/BMBRep.2023-0021. PMID: 36977606.

Liang X, Ho MCW, Zhang Y, Li Y, Wu MN, Holy TE, Taghert PH. 2019. Morning and Evening Circadian Pacemakers Independently Drive Premotor Centers via a Specific Dopamine Relay. *Neuron* 102. doi:10.1016/j.neuron.2019.03.028

Liu S, Liu Q, Tabuchi M, Wu MN. 2016. Sleep drive is encoded by neural plastic changes in a dedicated circuit. *Cell* 165. doi:10.1016/j.cell.2016.04.013

Luan H, Peabody NC, Vinson CR, White BH. Refined spatial manipulation of neuronal function by combinatorial restriction of transgene expression. Neuron. 2006 Nov 9;52(3):425-36. doi: 10.1016/j.neuron.2006.08.028. PMID: 17088209.

Meissner GW, Nern A, Dorman Z, DePasquale GM, Forster K, Gibney T, Hausenfluck JH, He Y, Iyer NA, Jeter J, Johnson L, Johnston RM, Lee K, Melton B, Yarbrough B, Zugates CT, Clements J, Goina C, Otsuna H, Rokicki K, Svirskas RR, Aso Y, Card GM, Dickson BJ, Ehrhardt E, Goldammer J, Ito M, Kainmueller D, Korff W, Mais L, Minegishi R, Namiki S, Rubin GM, Sterne GR, Wolff T, Malkesman O; FlyLight Project Team. A searchable image resource of *Drosophila* GAL4 driver expression patterns with single neuron resolution. Elife. 2023 Feb 23;12:e80660. doi: 10.7554/eLife.80660. PMID: 36820523.

Mertens I, Vandingenen A, Johnson EC, Shafer OT, Li W, Trigg JS, De Loof A, Schoofs L, Taghert PH. PDF receptor signaling in Drosophila contributes to both circadian and geotactic behaviors. Neuron. 2005 Oct 20;48(2):213-9. doi: 10.1016/j.neuron.2005.09.009. PMID: 16242402.

Nässel DR. 2009. Neuropeptide signaling near and far: how localized and timed is the action of neuropeptides in brain circuits? *Invert Neurosci* 9**,** 57-75. doi: 10.1007/s10158-009-0090-1.

Nässel DR. Substrates for Neuronal Cotransmission With Neuropeptides and Small Molecule Neurotransmitters in *Drosophila*. Front Cell Neurosci. 2018 Mar 23;12:83. doi: 10.3389/fncel.2018.00083. PMID: 29651236.

Nässel DR, Zandawala M. Recent advances in neuropeptide signaling in Drosophila, from genes to physiology and behavior. Prog Neurobiol. 2019 Aug;179:101607. doi: 10.1016/j.pneurobio.2019.02.003. Epub 2019 Mar 21. PMID:30905728.

Nern A, Pfeiffer BD, Rubin GM. Optimized tools for multicolor stochastic labeling reveal diverse stereotyped cell arrangements in the fly visual system. Proc Natl Acad Sci U S A. 2015 Jun 2;112(22):E2967-76. doi: 10.1073/pnas.1506763112. Epub 2015 May 11. PMID: 25964354.

Nern A, Loesche F, Takemura SY, Burnett LE, Dreher M, Gruntman E, Hoeller J, Huang GB, Januszewski M, Klapoetke NC, Koskela S, Longden KD, Lu Z, Preibisch S, Qiu W, Rogers EM, Seenivasan P, Zhao A, Bogovic J, Canino BS, Clements J, Cook M, Finley-May S, Flynn MA, Hameed I, Fragniere AM, Hayworth KJ, Hopkins GP, Hubbard PM, Katz WT, Kovalyak J, Lauchie SA, Leonard M, Lohff A, Maldonado CA, Mooney C, Okeoma N, Olbris DJ, Ordish C, Paterson T, Phillips EM, Pietzsch T, Salinas JR, Rivlin PK, Schlegel P, Scott AL, Scuderi LA, Takemura S, Talebi I, Thomson A, Trautman ET, Umayam L, Walsh C, Walsh JJ, Xu CS, Yakal EA, Yang T, Zhao T, Funke J, George R, Hess HF, Jefferis GS, Knecht C, Korff W, Plaza SM, Romani S, Saalfeld S, Scheffer LK, Berg S, Rubin GM, Reiser MB. Connectome- driven neural inventory of a complete visual system. bioRxiv [Preprint]. 2024 Jun 1:2024.04.16.589741. doi: 10.1101/2024.04.16.589741. PMID: 38659887.

Öztürk-Çolak A, Marygold SJ, Antonazzo G, Attrill H, Goutte-Gattat D, Jenkins VK, Matthews BB, Millburn G, Dos Santos G, Tabone CJ; FlyBase Consortium. FlyBase: updates to the Drosophila genes and genomes database. Genetics. 2024 May 7;227(1):iyad211. doi: 10.1093/genetics/iyad211. PMID: 38301657.

Park D, Veenstra JA, Park JH, Taghert PH. Mapping peptidergic cells in Drosophila: where DIMM fits in. PLoS One. 2008 Mar 26;3(3):e1896. doi: 10.1371/journal.pone.0001896. PMID: 18365028.

Parisky KM, Agosto J, Pulver SR, Shang Y, Kuklin E, Hodge JJ, Kang K, Liu X, Garrity PA, Rosbash M, Griffith LC. PDF cells are a GABA-responsive wake-promoting component of the *Drosophila* sleep circuit. *Neuron* 60: 672–682, 2008.

Pfeiffer BD, Ngo TT, Hibbard KL, Murphy C, Jenett A, Truman JW, Rubin GM. Refinement of tools for targeted gene expression in Drosophila. Genetics. 2010 Oct;186(2):735-55. doi: 10.1534/genetics.110.119917. Epub 2010 Aug 9. PMID: 20697123.

Pírez N, Christmann BL, Griffith LC. Daily rhythms in locomotor circuits in *Drosophila* involve PDF. *J Neurophysiol* 110: 700 –708, 2013.

Rubin GM, Aso Y. New genetic tools for mushroom body output neurons in *Drosophila*. Elife. 2024 Jan 25;12:RP90523. doi: 10.7554/eLife.90523.PMID: 38270577.

Scheffer LK, Xu CS, Januszewski M, Lu Z, Takemura SY, Hayworth KJ, Huang GB, Shinomiya K, Maitlin-Shepard J, Berg S, Clements J, Hubbard PM, Katz WT, Umayam L, Zhao T, Ackerman D, Blakely T, Bogovic J, Dolafi T, Kainmueller D, Kawase T, Khairy KA, Leavitt L, Li PH, Lindsey L, Neubarth N, Olbris DJ, Otsuna H, Trautman ET, Ito M, Bates AS, Goldammer J, Wolff T, Svirskas R, Schlegel P, Neace E, Knecht CJ, Alvarado CX, Bailey DA, Ballinger S, Borycz JA, Canino BS, Cheatham N, Cook M, Dreher M, Duclos O, Eubanks B, Fairbanks K, Finley S, Forknall N, Francis A, Hopkins GP, Joyce EM, Kim S, Kirk NA, Kovalyak J, Lauchie SA, Lohff A, Maldonado C, Manley EA, McLin S, Mooney C, Ndama M, Ogundeyi O, Okeoma N, Ordish C, Padilla N, Patrick CM, Paterson T, Phillips EE, Phillips EM, Rampally N, Ribeiro C, Robertson MK, Rymer JT, Ryan SM, Sammons M, Scott AK, Scott AL, Shinomiya A, Smith C, Smith K, Smith NL, Sobeski MA, Suleiman A, Swift J, Takemura S, Talebi I, Tarnogorska D, Tenshaw E, Tokhi T, Walsh JJ, Yang T, Horne JA, Li F, Parekh R, Rivlin PK, Jayaraman V, Costa M, Jefferis GS, Ito K, Saalfeld S, George R, Meinertzhagen IA, Rubin GM, Hess HF, Jain V, Plaza SM. A connectome and analysis of the adult Drosophila central brain. Elife. 2020 Sep 7;9:e57443. doi: 10.7554/eLife.57443. PMID: 32880371.

Schlegel P, Yin Y, Bates AS, Dorkenwald S, Eichler K, Brooks P, Han DS, Gkantia M, Dos Santos M, Munnelly EJ, Badalamente G, Serratosa Capdevila L, Sane VA, Fragniere AMC, Kiassat L, Pleijzier MW, Stürner T, Tamimi IFM, Dunne CR, Salgarella I, Javier A, Fang S, Perlman E, Kazimiers T, Jagannathan SR, Matsliah A, Sterling AR, Yu SC, McKellar CE; FlyWire Consortium; Costa M, Seung HS, Murthy M, Hartenstein V, Bock DD, Jefferis GSXE. Whole-brain annotation and multi-connectome cell typing of Drosophila. Nature. 2024 Oct;634(8032):139-152.doi: 10.1038/s41586-024-07686-5. Epub 2024 Oct 2. PMID: 39358521

Shafer OT, Kim DJ, Dunbar-Yaffe R, Nikolaev VO, Lohse MJ, Taghert PH. Widespread receptivity to neuropeptide PDF throughout the neuronal circadian clock network of Drosophila revealed by real-time cyclic AMP imaging. Neuron. 2008 Apr 24;58(2):223-37. doi: 10.1016/j.neuron.2008.02.018. PMID: 18439407.

Shafer OT, Keene AC. The Regulation of Drosophila Sleep. Curr Biol. 2021 Jan 11;31(1):R38-R49. doi: 10.1016/j.cub.2020.10.082. PMID: 33434488.

Shafer OT, Gutierrez GJ, Li K, Mildenhall A, Spira D, Marty J, Lazar AA, Fernandez MP. Connectomic analysis of the *Drosophila* lateral neuron clock cells reveals the synaptic basis of functional pacemaker classes. Elife. 2022 Jun 29;11:e79139. doi: 10.7554/eLife.79139. PMID: 35766361.

Shaw PJ, Cirelli C, Greenspan RJ, Tononi G. Correlates of sleep and waking in Drosophila melanogaster. Science. 2000 Mar 10;287(5459):1834-7. Doi: 10.1126/science.287.5459.1834. PMID: 10710313.

Sherer LM, Catudio Garrett E, Morgan HR, Brewer ED, Sirrs LA, Shearin HK, Williams JL, McCabe BD, Stowers RS, Certel SJ. Octopamine neuron dependent aggression requires dVGLUT from dual-transmitting neurons. PLoS Genet. 2020 Feb 25;16(2):e1008609. doi: 10.1371/journal.pgen.1008609. PMID: 32097408.

Sitaraman D, Vecsey CG, Koochagian C. 2024. Activity Monitoring for Analysis of Sleep in Drosophila melanogaster. *Cold Spring Harb Protoc*. doi:10.1101/pdb.top108095.

Svensson E, Apergis-Schoute J, Burnstock G, Nusbaum MP, Parker D, Schiöth HB. General Principles of Neuronal Co-transmission: Insights From Multiple Model Systems. Front Neural Circuits. 2019 Jan 21;12:117. doi:10.3389/fncir.2018.00117. PMID: 30728768.

Terhzaz, S., Rosay, P., Goodwin, S.F., Veenstra, J.A., 2007. The neuropeptide SIFamide modulates sexual behavior in *Drosophila*. *Biochem Biophys Res Commun* 352**,** 305-310.

Tirian L, Fellner M, Dickson BJ. 2017. The VT GAL4, LexA, and split-GAL4 collection for targeted expression in the *Drosophila* nervous system. bioRxiv. DOI: https://doi.org/10.1101/198648.

Turner-Evans DB, Jayaraman V. The insect central complex. Current Biology. 2016;26(11):R453–R457. PMID:27269718.

Tuthill JC, Nern A, Holtz SL, Rubin GM, Reiser MB. Contributions of the 12 neuron classes in the fly lamina to motion vision. Neuron. 2013 Jul 10;79(1):128-40. doi: 10.1016/j.neuron.2013.05.024. PMID: 23849200.

Vecsey CG, Koochagian C, Porter MT, Roman G, Sitaraman D. 2024. Analysis of Sleep and Circadian Rhythms from Drosophila Activity-Monitoring Data Using SCAMP. *Cold Spring Harb Protoc*. doi:10.1101/pdb.prot108182

Wiggin TD, Goodwin PR, Donelson NC, Liu C, Trinh K, Sanyal S, Griffith LC. 2020. Covert sleep-related biological processes are revealed by probabilistic analysis in Drosophila. *Proc Natl Acad Sci U S A* **117**. doi:10.1073/pnas.1917573117.

Wohl MP, Liu J, Asahina K. Drosophila Tachykininergic Neurons Modulate the Activity of Two Groups of Receptor-Expressing Neurons to Regulate Aggressive Tone. J Neurosci. 2023 May 10;43(19):3394-3420. doi: 10.1523/JNEUROSCI.1734-22.2023. Epub 2023 Mar 28. PMID: 36977580.

Wolff T, Rubin GM. Neuroarchitecture of the Drosophila central complex: A catalog of nodulus and asymmetrical body neurons and a revision of the protocerebral bridge catalog. J Comp Neurol. 2018 Nov 1;526(16):2585-2611. doi: 10.1002/cne.24512. Epub 2018 Oct 18. PMID: 30084503.

Wolff T, Iyer NA, Rubin GM. Neuroarchitecture and neuroanatomy of the Drosophila central complex: A GAL4-based dissection of protocerebral bridge neurons and circuits. J Comp Neurol. 2015 May 1;523(7):997-1037. doi:10.1002/cne.23705. Epub 2014 Dec 16. PMID: 25380328.

Wu F, Deng B, Xiao N, Wang T, Li Y, Wang R, Shi K, Luo DG, Rao Y, Zhou C. A neuropeptide regulates fighting behavior in *Drosophila melanogaster*. Elife. 2020 Apr 21;9:e54229. doi: 10.7554/eLife.54229. PMID: 32314736.

Wu M, Nern A, Williamson WR, Morimoto MM, Reiser MB, Card GM, Rubin GM. Visual projection neurons in the *Drosophila* lobula link feature detection to distinct behavioral programs. Elife. 2016 Dec 28;5:e21022. doi: 10.7554/eLife.21022. PMID: 28029094.